FLOW BATTERY DESIGN FOR A JELLYFISH ROBOT

A Thesis

Presented to the Faculty of the Graduate School

of Cornell University

In Partial Fulfillment of the Requirements for the Degree of

Master of Science

by

Xu Liu

August 2020

ABSTRACT

The use of a rigid battery-based energy storage system is among one of the most important limitations to soft robots. First, the non-stretchable parts in rigid secondary batteries severely limit the range of adaptation or flexibility of the robots. Second, to achieve more prolonged operation for soft robots, a higher mass will be required for the rigid battery system—which creates additional problems such as being over-weight. In the current study, we introduce a new multi-functional energy storage system for a jellyfish soft robot. We solve the problem for traditional rigid batteries by inventing a multi-functional redox flow battery (RFB) system to realize energy storage and tendon-fluid scheme simultaneously. The RFB system exhibits excellent flexibility for the minimum rigid components inside. Electricity is produced by ion exchange between two membrane-separated chemical liquids, and the fluid-based energy storage can be multi-purposed for actuation or structure. We use RFBs for the controllable stiffening of tentacles, which works as the tendon for the swimming of the robot. In this thesis, we introduce three design iterations for the ZnI_2 flow battery system and demonstrate the untethered swimming for the fluid-tendon of the flow-battery robot jellyfish out of 3D printed parts and polymer films. We also investigate the effect of graphite felt electrode compression on porosity, resistance, and battery performance. The use of ethanol as an organic additive to minimize dendrite formation is also studied. We have successfully validated the use of flow batteries can facilitate increased efficiency, energy density, and multifunctionality for a jellyfish soft robot.

BIOGRAPHICAL SKETCH

Xu Liu was born in Qufu, Shandong Province, China. She joined Prof. Robert Shepherd's group in August 2018 and focused on the projects of flow battery design for soft robots. Before coming to Cornell, she graduated from the University of British Columbia in Vancouver, BC, Canada in 2018, and Xi'an Jiaotong University in 2016.

In 2020, she was one of the fifty people from around the world to receive the German Chancellor Scholarship Program (declined due to Ph.D. study at Cornell), an initiative by the Alexander Von Humboldt Foundation. She was among the "AACYF Top 30 Under 30 Elites" (30 in the US) in "Art, Culture, Entertainment, Science" by All America Chinese Youth Federation. Meanwhile, she was selected into the Clinton Global Initiative University by the Clinton Foundation. She was named as a Local Pathways Fellow by the UN SDSN–Youth (2020-2021), and received the National Scholarship (Top 0.2%) by the Ministry of Education China (2015).

In 2019, Xu was featured by BP plc as a Future Energy Leader (11 in the world). Xu has published two first-authored journal articles and has been serving as a referee for the *International Journal of Hydrogen Energy* and the *IEEE Robotics and Automation Letters*.

ACKNOWLEDGMENTS

First, I would like to say thanks to my advisor, Prof. Robert Shepherd, who is a huge supporter during my M.S. study at ORL. The incredible project and academic freedom in ORL are what motivates me to continue my Ph.D. study at Cornell. I would like to express my gratitude for having the opportunity to collaborate with Prof. Lynden Archer's group. I also want to thank Prof. David Erickson for agreeing to be my committee member and thanks for sending so many reference letters on my behalf! Especially, I am very grateful to my colleagues in ORL who are working with me on the same projects, Autumn Pratt, Dr. Hyeon Seok An, and Matthew Daniel for their generous help throughout this project.

I want to express my gratitude to all my other colleagues in ORL. I cherish the great memories of working with Dr. Anand Mishra, Dr. Yoav Matia, Shuo Li, Patricia Xu, Jose Barreiros, Lillia Bai, Cam Aubin, Cameron Burkey, Wenjiong Gu, Kaiyang Wang. I also appreciate my lovely officemates, Maura Neill, Rachel Miller, Emilie Baker, and Ronald Heisser (yes, you should feel lucky to be in the same office with four ladies). Working with them is such an enjoyable journey in my life. Luckily, I will continue my research as a Ph.D. in our lab, which gives me more years to work with them (hopefully not that many years).

I would like to thank my family members in China, especially my parents, for their unconditional love for me. I am so proud of them and will cherish their love.

TABLE OF CONTENTS

List of Figures

List of Tables

1. Introduction

1.1 Research Background and Significance

Since the beginning of the 21st century, robots have widely been used in medical, industrial, exploratory, and many other applications. For traditional robots, they are mostly composed of rigid kinematic joints based on hard materials (metal, plastic, etc.), which can complete fast, accurate, and repeatable position or force control tasks[1-5]. However, this kind of robot has limited movement flexibility, low environmental adaptability, and can only work in a structured environment[6-8]. These shortcomings limit the application of robots in dynamic, unknown, and unstructured complex situations, such as military surveillance, disaster rescue, and scientific detection.

To increase the moving ability for rigid robots, researchers have been exploring different pathways, such as by increasing the degree of freedom for rigid robots so that they have a certain degree of continuous deformation ability, forming a hyper-redundant robot. Compared with traditional rigid robots, the environment adaptability for this kind of robot has improved[9-11]. However, its body is still composed of hard materials, the size of which cannot be changed arbitrarily. When applied in a specific environment, we have to provide a priori environmental information such as the shape and size of obstacles, which sets limitations for practical applications.

Nature has already had well-established systems (e.g., mollusks) to solve the adaptability issue[12-16]. Mollusks are widely distributed in seawater, freshwater, and land. After millions of years in natural optimization, the soft tissue of this animal has combined advantages of lightweight, high power density ratio, and high endurance for large deformations. They can exercise efficiently under complex natural environmental conditions by changing their body shape. In recent years,

researchers have used mollusks as prototypes for designing soft robots[17, 18]. This robot is made of flexible materials. Through precise design, it can continue to deform and can withstand large strains. By simulating the morphological structure of living things, it can crawl, twist, and creep through small spaces and realize grasping and other operations. It has a wide range of applications in unstructured environments. Compared with super-redundant robots made of hard materials, soft robots have very little resistance to pressure and can be compatible with obstacles by compliant deformation. This can significantly reduce the contact force so that the soft robot can carry delicate or fragile items.

Figure 1.1 Examples of soft robots[17, 18].

Different from the traditional robots that rely on motor drives, the driving method of soft robots mainly depends on the smart materials being used. Generally, they can be classified into the following categories: dielectric elastomer (DE)[19-21], ionic polymer-metal composite (IPMC)[22], shape memory alloy (SMA)[23, 24], shape memory polymer (SMP)[25], etc. The physical input from the response can be divided into the following types: light[26], temperature[27], pressure[28], electric field[29], magnetic field[30], and chemical reaction[31]. Accordingly, scientists have designed a variety

of soft robots, mostly by imitating various creatures in nature, such as earthworm[32, 33], octopus[34, 35], and jellyfish[36, 37].

1.2 Traditional Energy System in Robotics

One of the critical components of robots is their energy system. In this section, we will go over the traditional energy systems (i.e., chemical batteries) currently being used in robotics. According to whether the system is rechargeable, chemical batteries can be classified into primary and secondary types[38] (also known as storage batteries or rechargeable batteries). The latter kind of batteries can be reused multiple times. The most commonly used secondary batteries in robotic systems include nickel-cadmium batteries, nickel-metal hydride batteries, lithium-ion/lithium polymer batteries, and lead-acid batteries. In 1.2.1 and 1.2.2, we will describe one primary battery (i.e., dry cell battery) and one secondary battery (e.g., lead-acid battery) in detail, respectively.

Figure 1.2 Dry cell battery and lead-acid battery.

1.2.1 Dry Cell Battery

Dry cell batteries are primary batteries, and they have evolved into a large family. Till now, there have been over a hundred kinds of dry cell batteries. Conventional dry cell batteries include ordinary zinc-manganese batteries, alkaline zinc-manganese batteries, magnesium-manganese

batteries, zinc-air batteries, zinc-mercury oxide batteries, zinc-silver oxide batteries, lithium-manganese batteries, etc.

Zinc-manganese dry cell batteries are among the most used ones. Due to structural differences, they can be further classified into the following types: paste zinc-manganese, cardboard zinc-manganese, film-type zinc-manganese, zinc chloride-manganese, alkaline zinc-manganese, laminated zinc-manganese, and four-pole parallel zinc-manganese dry batteries, to name a few.

Dry batteries are costly in practical applications, partly due to their high internal resistance. For example, the internal resistances of ordinary zinc-manganese batteries or alkaline batteries usually fall between the range of 0.5 to 10 ohms. Therefore, when there is a load being added, the voltage drop is swift, making the robot unable to keep continuous operation under a large current. Thus, dry cell batteries are not ideal power sources for robotic systems.

1.2.2 Lead-acid Battery

Lead-acid batteries are secondary batteries. The system usually consists of PbO_2 as the anode, Pb as the cathode, and H_2SO_4 solution as the electrolyte in between. The anode (PbO_2) and the cathode (Pb) are immersed in the electrolyte (dilute H_2SO_4), and 2 V of voltage can be generated when discharging happens between the two electrodes. The reactions during the discharging process are[39]:

Negative plate reaction:

$$Pb\ (s) + HSO_4^-\ (aq) \longrightarrow PbSO_4\ (s) + H^+\ (aq) + 2e^- \qquad \text{(Eqn 1)}$$

Positive plate reaction:

$$PbO_2\ (s) + HSO_4^-\ (aq) + 3H^+\ (aq) + 2e^- \longrightarrow PbSO_4\ (s) + 2H_2O\ (l) \qquad \text{(Eqn 2)}$$

When the battery is connected to an external circuit, during discharging, dilute sulfuric acid will react with the active materials on the cathode and anode plates to form a new compound, lead sulfate. The longer the discharging process, the lower the sulfuric acid concentration will be. The consumption of sulfuric acid is proportional to the discharging energy of the battery. By measuring the concentration of sulfuric acid in the electrolyte (i.e., the specific density), we can estimate the discharge capacity or the residual capacity of the battery system.

During the charging process, the lead sulfate generated on the anode and cathode plate during discharging will be decomposed and reduced to sulfuric acid, lead and lead peroxide, so that the concentration of sulfuric acid in the battery will gradually increase and return to its initial level before discharging. The active materials in the battery system will then be restored to a state where it can be powered again. When the lead sulfate at the two electrodes is reduced to the initial concentration, the charging process ends. If the lead-acid battery is overcharged, the water in the electrolyte will be split; thus, more water needs to be added to the system.

The most significant advantage of lead-acid batteries is their low price, and the ability for discharging under a high current density of above 20 C (i.e., 10 Ah batteries can achieve a discharge current of 10*20 = 200 A). The other advantages include the strong tolerance for overcharging, high system reliability, and the ease in charging and discharging control. The

principal disadvantage, however, is the low lifetime, and the charge and discharge cycles usually cannot exceed 500 times. The high mass of the system also makes it difficult to maintain.

1.3 Design Considerations for the Energy System of Soft Robots

In the design of robots, the energy system is particularly important. Usually, we choose the appropriate battery according to the weight and volume of the robot and the power consumption of the electronic devices in the robot. The mass of the battery itself can also account for a large proportion of the robot's weight; thus, a significant amount of the battery energy needs to be consumed to sustain itself.

On the one hand, energy storage is one of the main barriers for robots to automate. Usually, robots use rigid batteries, and the most direct way to achieve higher power is by adding more cells together. However, the increase in the number of batteries will inevitably lead to unbalanced robot weight. Therefore, the robot needs to be redesigned to maintain its balance and performance. On the other hand, energy storage is also one of the limiting factors for the autonomy of robotic systems. Merely increasing the number of batteries will lead to the rising weight and volume of the robot, and a more robust support system and joints are needed to support its weight, hindering the long-duration autonomy for the robotic system[40].

Scientists have been trying to solve the problem by the adoption of a multi-functional system that decreases the weight of the robot by enabling different functions into one system. Choi's group designed heavy lead-acid batteries that are used for weight balancing in electric forklifts through a phase shift full-bridge converter with a current doubler[41]. Liu developed lithium-ion batteries

with elastic or potential structural load-bearing capabilities with an energy density of 35 Wh/kg[42]. Wetzel's group designed and fabricated a multi-functional battery system by modifying polymer electrolytes. This system could change its conductivity and stiffness by spanning continuously[43]. In the context of soft robotics, the multi-functional batteries listed above are still not ideal, due to their rigid components inside. Therefore, the direction is to make all parts of the robots soft to increase flexibility and adaptability while accomplishing tasks[44-48]. This can make sure the safety of people when touching or working around the robot. Apart from that, another direction is to make the batteries dynamic and not static, which provides us more opportunities to tap its potential in different functions.

The current work builds upon the previous efforts by our group in a vascular system for a robot fish. The vascular flow battery is pumped through the fish to power the artificial muscles that cause the fish to swim. By adding the flow battery, the fish can swim for 400% longer than it could without this vascular system. The flow batteries alone, however, are not sufficient for the energy need for the whole system, and lithium batteries are still needed as the additional energy source to power the electric modules, and the peristaltic pump to circulate the electrolyte of the cell[40].

All the work mentioned above has inspired us to develop a flow battery system with a high energy density for applications in a jellyfish soft robot. Flow batteries, as the name denotes, can store energy in the liquid form, and have the potential to be used in the soft robot for its quick response, safety, and design flexibility[49-55]. Designing a flow battery system with tendon driven fluidic structures enables us to make a multi-functional fluid energy storage that can help create longer-

operating robots. Meanwhile, for soft robots, fluid energy storage can be multi-purposed for actuation or structure.

1.4 Redox Flow Battery

1.4.1 Introduction of Redox Flow Batteries

Redox flow batteries, unlike traditional energy systems (i.e., chemical batteries), have the promise to be adapted into soft robotic systems, due to its "soft" nature when compared with traditional rigid systems.

L. H. Thaller first proposed the concept of the flow battery in 1974[56]. The battery realizes the conversion of electrical energy and chemical energy through the reversible redox reaction of the active materials in anolyte (or posolyte) and catholyte (or negolyte). During charging, the positive electrode is oxidized, and the valence of the active material increases. The negative electrode undergoes a reduction reaction, and the valence state of the active material decreases. The discharge process is the opposite. Different from rigid batteries, anolyte and catholyte are stored in an external tank of the flow battery. They are then pumped inside the battery system via a tubing system. Therefore, the power and capacity of the battery can be adjusted separately[57, 58].

The active material of a conventional secondary battery is generally integrated with its electrode material. The separator between the positive and negative electrodes is a porous insulating membrane, and there are usually phase changes or morphological changes during charging and discharging. After the battery output power is fixed, its energy storage capacity is also set accordingly. In structure, flow battery systems are entirely different from the traditional secondary

batteries. Flow batteries are mainly composed of a seperator, anolyte and catholyte, the tank for electrolyte storage, a battery management system, a charge and discharge setup, and an energy storage monitoring system[59, 60]. The stack is central to the energy storage system for the flow battery and is generally formed by dozens of single batteries being pressed in the form of a filter[61]. Therefore, the structure of the flow battery is similar to the fuel cell stack with a proton exchange membrane.

1.4.2 Flow Battery Unit

Flow battery cells are the most basic unit for evaluating battery materials and components, optimizing battery structural design and operating conditions, and assembling stacks. As shown in Figure 1.3, at the center of the unit cell is a conductive membrane that separates the anolyte and catholyte, and conducts protons/ions to form a current loop. Electrodes, electrode frames, sealing o-rings, bipolar plates, current collecting plates, insulating plates, end plates, etc., are symmetrically arranged on both sides of the separator[62].

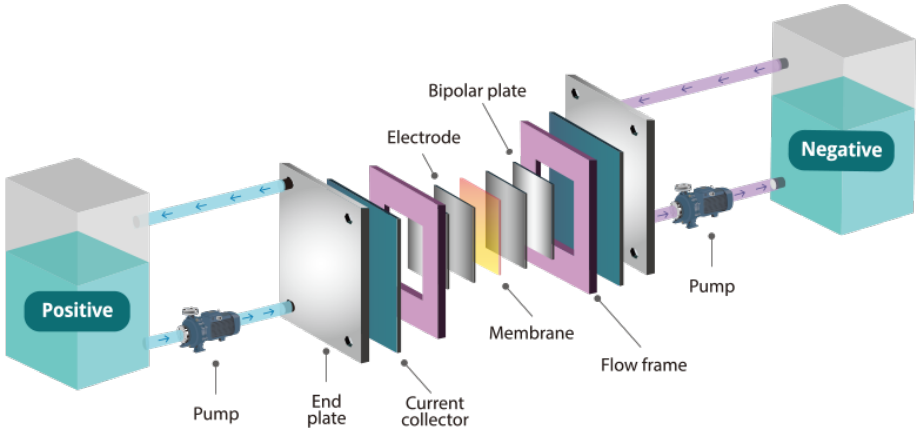

Figure 1.3 Schematic of the components of a flow battery unit[62].

1.4.3 Flow Battery Stack

The seperator is the main component of the flow battery system. As shown in Figure 1.4, the seperator is composed of multiple cells in a superimposed manner. It consists of circulation pipes of electrolyte solution sharing by various cells, with a uniform current output. The performance and cost of the stack directly affect the whole flow battery system. The focus of the research in recent year includes reducing the concentration polarization loss, as well as improving the efficiency and even distribution of the electrolyte solution in every single cell. The alternative approaches to improve the efficiency of the battery include improving the surface reaction activity for the electrode, minimizing the ohmic polarization loss, and reducing the activation polarization loss as well as the internal resistance of the stack. In addition, it is necessary to design an effective sealing structure and an effective assembly process to improve the production efficiency and operational reliability of the stack[63].

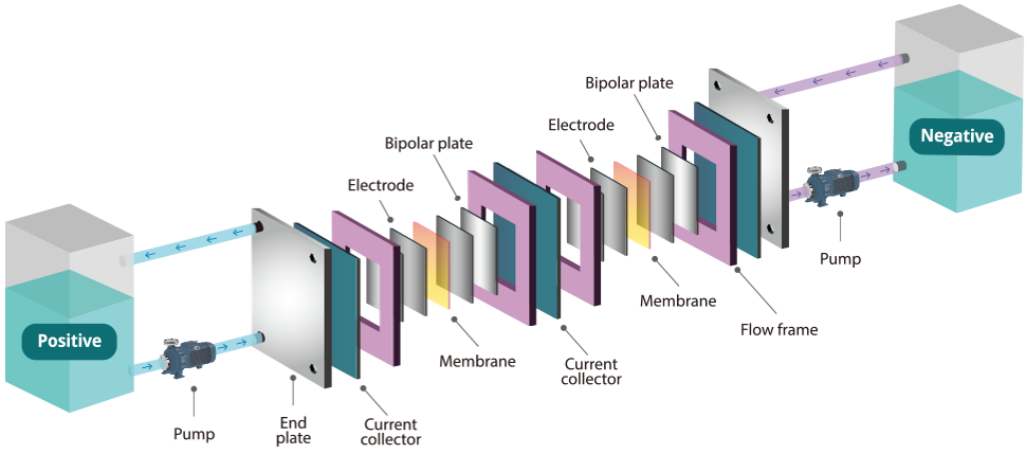

Figure 1.4 Schematic of the components of a flow battery stack[62].

1.4.4 Classification of Flow Batteries

According to the active material pairs, flow batteries can be classified into zinc/bromine[64-66], zinc/chlorine[67-69], zinc/cerium[70, 71], zinc/nickel[72, 73], sodium polysulfide/bromine[74, 75],

iron/chromium[76, 77], and vanadium flow batteries[78, 79]. Based on the phase of anolyte and catholyte active materials, flow batteries can be divided into classical and hybrid flow batteries[60].

In standard flow batteries, the anolyte and catholyte solutions are both water-soluble. These include all-vanadium, sodium polysulfide/bromine, iron/chromium, and multi-halide flow batteries.

The hybrid type flow battery refers to a flow battery with a deposition reaction during operation. Based on the reaction characteristics, it can be further divided into semi-deposition type and full-deposition type. The former only has the deposition reaction on either the anolyte or the catholyte solutions (thus also called single flow batteries), and typical examples include zinc/bromine and zinc/nickel flow batteries. The latter refers to a system where deposition reaction happens in both the anolyte or the catholyte solutions, and examples include chromic acid flow batteries.

Table 1.1 shows different flow batteries. The characteristics and examples of several typical flow batteries are introduced in detail below.

Table 1.1 Classification of redox flow batteries.

Classification	Characteristic	Example
Classical flow battery	Same species in both half-cells	All-vanadium flow battery
	Different species in each half-cell	Fe-Cr flow battery
Hybrid flow battery	Solid reactant or product at one electrode	Zn-Br_2 flow battery
	Both electrodes involve solid phases	Soluble Pb flow battery
	H_2 or O_2 related	Zn-air flow battery

1.5 Hypothesis and Objective

Researchers have studied different energy storage systems for soft robots. However, most of the energy storage systems are based on solid batteries. This has limited soft robots from adapting or changing shapes to meet specific requirements. In contrast, flow batteries have minimum rigid internal components. The fundamental design of flow batteries allows them to deliver varying power or energy for the specific task to be accomplished. The movement of the liquid electrolyte in the flow battery allows for a smoother and higher degree of motion for the soft robot. These characteristics of the flow batteries enable soft robots to adapt to the task to be accomplished. However, the application of flow batteries in the field of soft robotics is still in a very early stage. In this study, we will design and fabricate a jellyfish robot driven by the flow battery. The objectives of the project are (i) to develop the compatible flow battery system based on the specific shape of the jellyfish robot, and (ii) to improve the electrochemical performance of the flow battery. Our specific aims include:

1. We will manufacture the untethered swimming fluid-tendon for the jellyfish robot out of 3D printed parts and polymer films.
2. In Chapter 2, we will describe the three design iterations for the flow battery system and show the detailed steps for battery preparation, electrode modification, and electrochemical characterization of thin films. The ZnI_2 flow battery system can be used as the power supply for the jellyfish robot. The hexagonal fluidic network architecture will also be built for variable stiffness control.

3. In Chapter 3, we will conduct a theoretical calculation to determine the maximum swimming duration with the flow battery system as described, and compare its energy density with that of traditional energy systems.
4. In Chapter 4, we will examine the effect of compression ratios of the graphite felt electrode on porosity, resistance, and the electrochemical performance for the flow battery system.
5. In Chapter 5, we will explore the optimized ratio of using ethanol as an organic additive to achieve maximum inhibition on dendrite growth.

2. Flow Battery Design and Experimental Methods

2.1 The Choice of Flow Battery System

On land, a robot has to support its own weight, making it difficult to get competitive movement abilities for a land-based robot powered by flow batteries. However, in water, a neutrally buoyant robot does not need to support the weight of its own. This will make competitive motion abilities more easily achievable. Flow battery robots are most likely to be competitive as swimming robots, rather than walking robots. Thus, in our project, a jellyfish robotic system was chosen as a good module to realize the multi-functional for the flow batteries, since the similar density between electrolyte and water will provide enough buoyancy for the jellyfish to float in the water.

For the battery, the zinc iodine redox flow battery (RFB) system was studied in the present work, due to its high energy density and low cost. Zinc-bromine RFB is also well established, but the toxic and corrosive nature of bromine hinders its practical applications[51]. Iodide, on the other hand, is non-toxic, highly reactive, soluble, and reversible, thus is deemed as a promising redox-active species for RFBs.

The working principle of the ZnI_2 RFB is shown in Figure 2.1. ZnI_2 works as both anolyte and catholyte in the battery before charging. During charging, I^- is oxidized to form iodine (I_2) on the positive electrode. I_2 is insoluble in water but will react with remaining I^- in the electrolyte to create I_3^-. I_3^- ions will be the primary substance in the solution. Since I_3^- has a fast charge transfer rate during the reduction reaction, the primary reaction in the ZnI_2 RFB occurs between I_3^- and I^-. On the negative electrode, Zn^{2+} undergoes a reduction reaction, and the resulting metal zinc is

deposited on the negative electrode surface. In the ZnI_2 solution, the primary reactions on the electrode are as follows:

Anode:

$$3I^- - 2e^- \leftrightarrow I_3^- \quad \text{(Eqn 3)}$$

Cathode:

$$Zn^{2+} + 2e^- \leftrightarrow Zn \quad \text{(Eqn 4)}$$

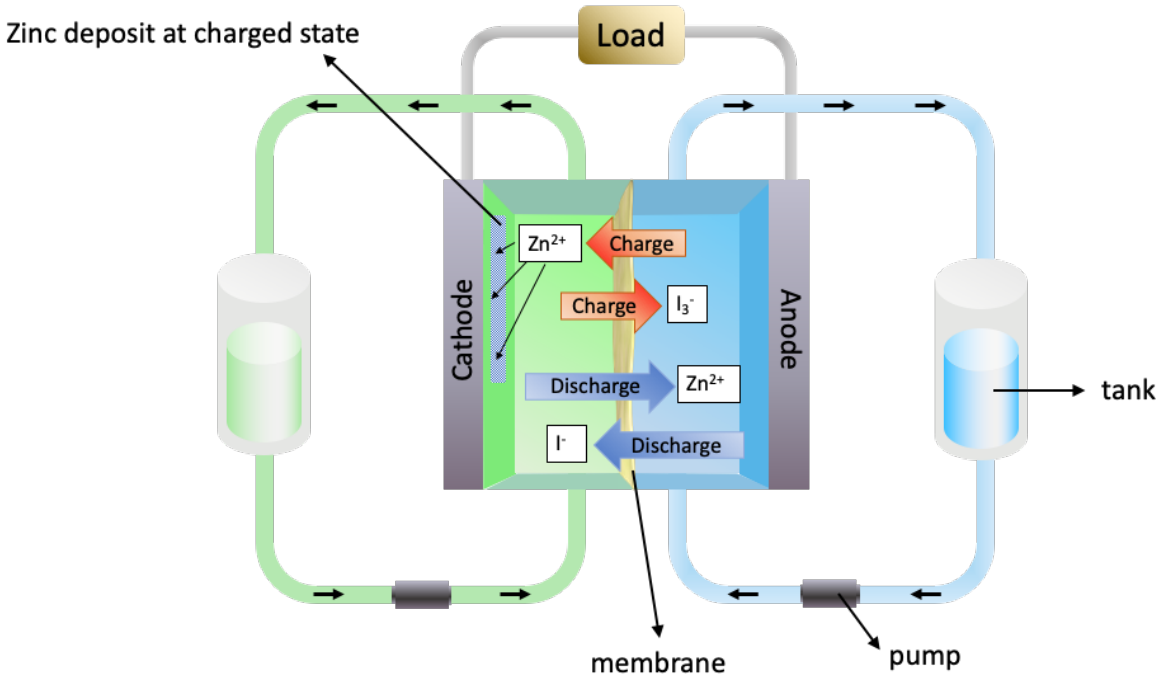

Figure 2.1 Schematic of the zinc iodide flow battery.

Based on the reaction potential on both electrodes, the total voltage of ZnI_2 RFB is determined as 1.29 V. The theoretical power output of the flow battery changes with the electrolyte concentration. The theoretical capacity of the flow battery can be calculated based on the equation below:

$$Q = nFM \quad \text{(Eqn 5)}$$

where Q is the charge of an electron transfer reaction, n represents the number of electrons involved in the redox reaction, and F denotes the Faraday constant (96,485 C/mol). If we assume the concentration of the electrolyte is 1 M, then n should 2 for the zinc/iodide reaction. After calculation, the charge transferred in the reaction is 128666 coulombs, that is, 35.74 Ah. Therefore, the theoretical capacity of the battery should be 111.96 mAh/g for ZnI_2 RFBs. We can conclude that the theoretical capacity of the battery will not change with the concentration or volume of the solution.

Previous studies show that for ZnI_2 RFBs, Zn^{2+} will pass through the Nafion membrane in the form of $[Zn{\cdot}6H_2O]^{2+}$ from the negative to the positive electrode during the charging process[52]. Therefore, during charging, zinc ion concentration will rise at the positive electrode, and stay constant on the other side. For ZnI_2 RFBs, anolyte concentration is the only factor affecting the system's energy density, and catholyte was not directly involved with the redox reactions. Thus, it possible to remove catholyte from the battery. This also inspires the design of the battery for the jellyfish robot.

Limited by the narrow space inside of the jellyfish robot, the ZnI_2 RFB is the ideal choice due to its high energy density and the feasibility in electrolyte design, as analyzed above. However, the system design needs to be more compatible and multi-functional to be able to adapt to the specific soft robotic systems. We will talk about the three design iterations in the following section.

2.2 The Design of Flow Battery in the Jellyfish Robot

As shown in Figure 1.3, the main components of a conventional flow battery include electrodes, current collector, ion exchange membrane, pump, electrolyte, and connecting tubes. The principal

objective of our project is to design the flow battery compatible for applications in the jellyfish robot and apply a tendon-fluid scheme to the battery.

2.2.1 First Generation

Figure 2.2 shows the first generation of flow battery design for the jellyfish robot. To increase the reaction area of the flow battery, we integrated and connected two flow batteries in parallel. To ensure that the electrolyte could penetrate smoothly and circulate inside the electrode, we selected carbon cloth as the electrode. As shown in Figure 2.3a, we printed a holder with a 7 cm diameter opening in the middle with Elastomeric Polyurethane (EPU) to support the carbon cloth. On each side of this holder were the two electrodes and the Nafion membrane. Next to the inside of the holder, a piece of carbon cloth was bound by stainless steel wire, which acted as a current collector to conduct electrons to the robot (Figure 2.3b). Zn powders were coated on the carbon cloth of the negative electrode to facilitate the reaction (Figure 2.3c). After drying, we glued the edge of Nafion to separate the positive and negative electrolytes on both sides of Nafion (Figure 2.3d). Afterward, another piece of carbon cloth electrode was tied to the outside of Nafion, by stainless steel passing through the middle hole on the holder. At the same time, we insulated the stainless steel wires to prevent short circuits in the electrolyte (Figure 2.3e). Eight tentacles were evenly distributed in the lower part of the cavity (Figure 2.3f). The middle space of the two layers of Dragon Skin can be used for storing electrolyte, and the electrolyte could freely communicate between the cavity and the tentacles. At the bottom of the cavity were the mechanical control and drive modules, including motors and the control board, which controlled the jellyfish robot to start and swim.

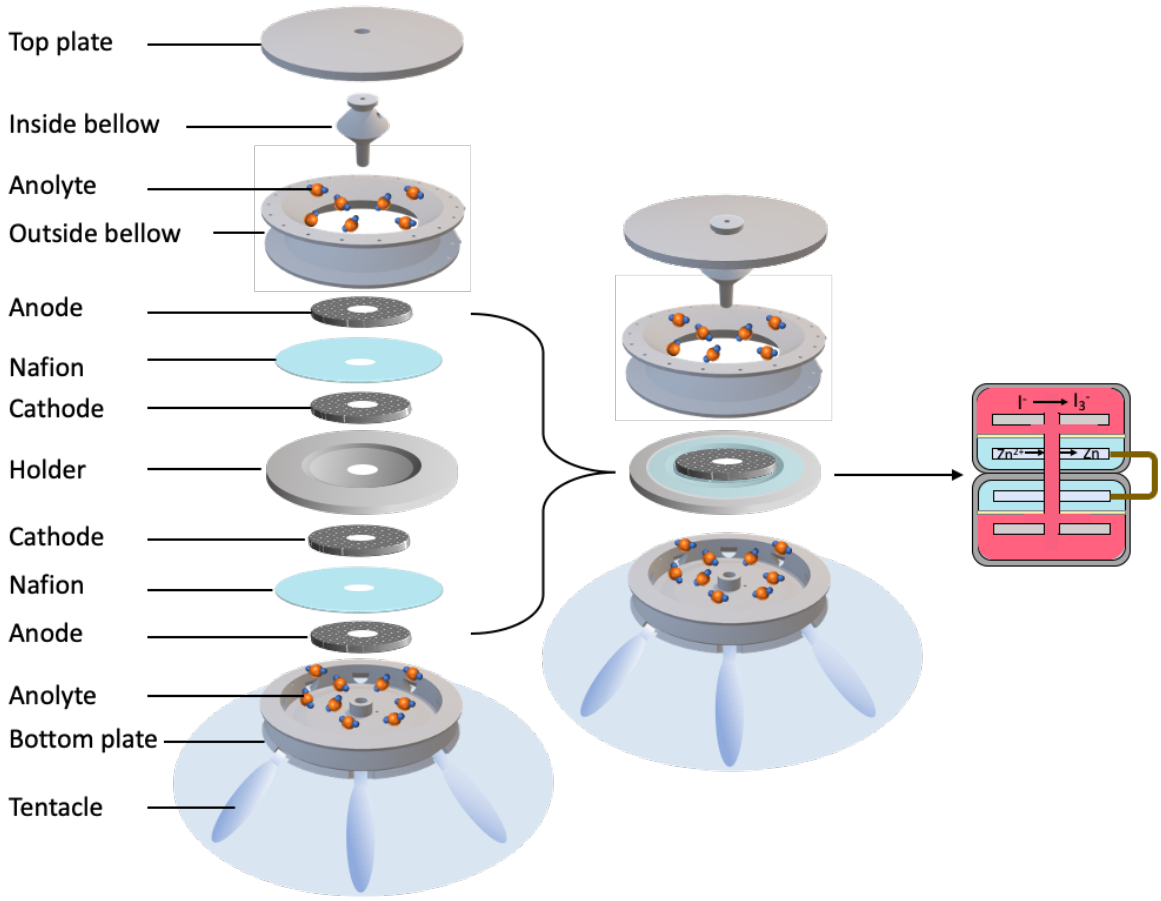

Figure 2.2 Assembly of the first generation jellyfish robot.

Overall, with the holder as the demarcation object, flow batteries were formed on both sides. Since the stainless steel wire was threaded up and down through the holder to tie two pieces of carbon cloth close to the holder, the two parts of carbon cloth were conducted. In this way, the two batteries were connected in parallel.

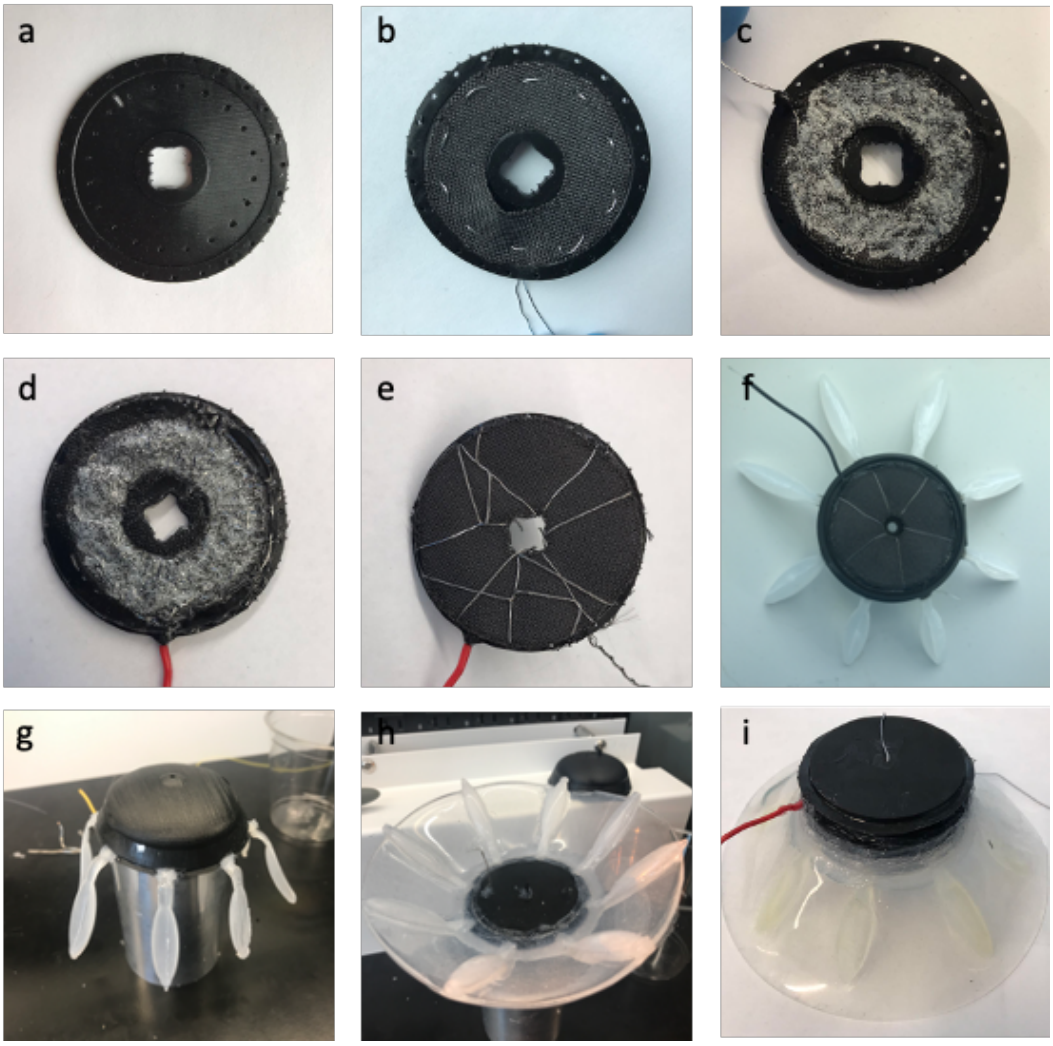

Figure 2.3 The assembling process of the jellyfish robot.

The jellyfish robot was made out of 3D printed parts and polymer films. Most components of the flow battery were printed in EPU, while the outside and inside bellows were printed in SIL. SIL is a flexible material that can promote electrolyte flow by extrusion. One bellow printed in SIL was placed in the middle of the chamber. After compression, it could rebound strongly to its original shape. Meanwhile, the tentacles were made with Dragon Skin 30, a stretchable material to form a chamber for the electrolyte. This design effectively guaranteed the regular compression of the robot cavity and provided continuous force for the flow of the electrolyte.

When the battery was fully charged, it would power the motor at the bottom of the jellyfish robot. When the motor pulled the tendon isolated from the electrolyte by the bellow through the holder's central hole, the outside bellow in the central part of the robot would be squeezed. The electrolyte passed through the hole in the holder's center from the cavity's upper part to the lower section and finally flowed into the tentacles of the robot. As a result, the tentacles increased stiffness and were pulled by another motor to toggle water. This enabled the robot to swim forward. After that, the motor rotated in reverse, and the tendon was loosened. The robot's cavity rebounded to its original shape due to the bellow's elasticity, and the electrolyte flowed back into the cavity from the tentacles.

Through the battery test, we found that the battery of the above design often failed to charge and discharge regularly, possibly due to the following reasons. First, for flow batteries, the flow rate of electrolyte in the electrode material plays an important role. A higher flow rate facilitates electrolyte renewal and speeds up the reaction rate. Generally, the flow rate of the electrolyte will not increase indefinitely, which is limited by the fact that the pump driving the liquid flow consumes more power at high flow rates. Since carbon cloth had a low surface area and was placed close to the holder, the electrolyte was more likely to flow in the space where the resistance was lower than that of the carbon cloth. This resulted in a low flow rate of the electrolyte inside the carbon cloth. In the carbon cloth, the reactants continued to increase but failed to flow away on time. This caused the overpotential to grow to a level that the battery could not be charged and discharged. Second, when the positive electrode was sealed by Nafion, to ensure the glue's effectiveness, the positive electrode carbon cloth and Nafion must be dry. This made it difficult for the catholyte to reach the positive electrode through Nafion due to the low water content of

Nafion in the early stage of the reaction. Third, the glue sealing the electrode can easily shed off during charging, since Nafion would encounter water swelling. The anolyte and catholyte flowed and mixed through the gap at the edge of Nafion, leading to the battery being scrapped.

2.2.2 Second Generation

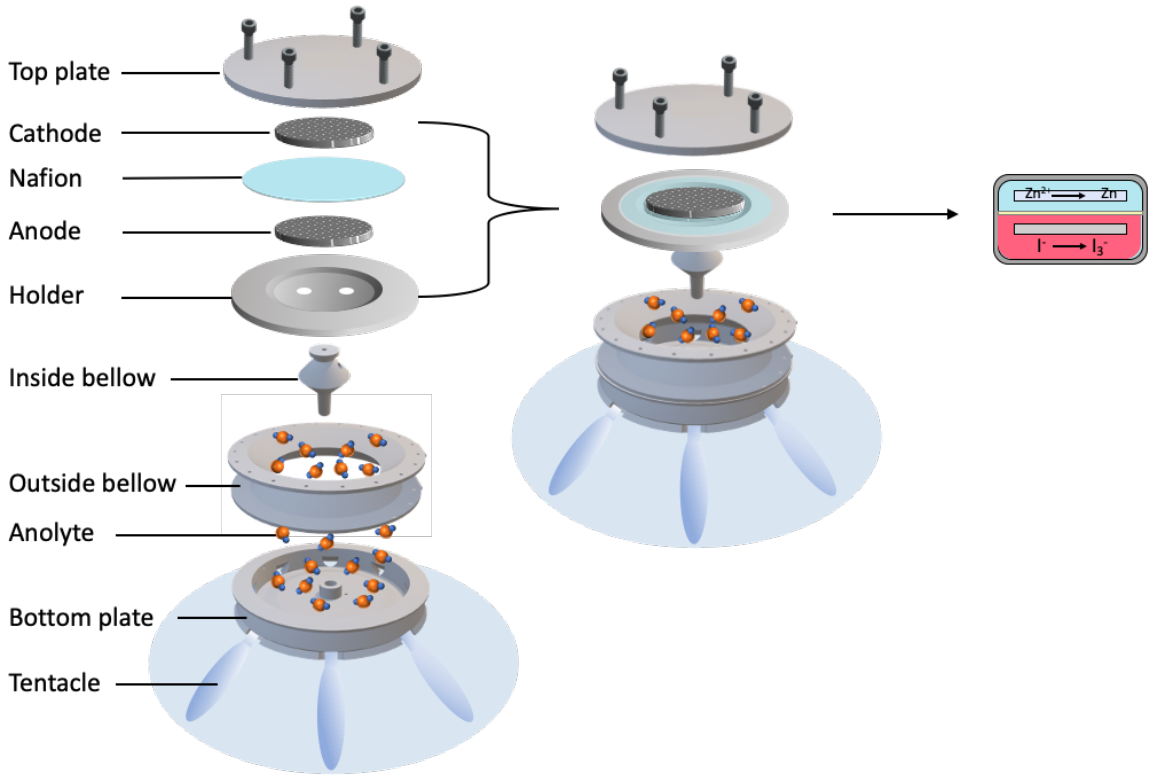

Figure 2.4 Assembly of the second generation jellyfish robot.

To solve the problem of the low surface area of carbon cloth, we replaced carbon cloth with graphite felt that has a diameter of 7 cm and a thickness of 3.2 mm. Since the resistance of graphite felt was higher than that of carbon cloth, it was compressed by two RPU plates to reduce the resistance. These two plates well sealed the separator of the battery. The stainless steel wire passed through the carbon felt as a current collector. Nafion was sandwiched tightly by the electrodes and O-ring. To ensure that the graphite felt was evenly compressed and reduce the complexity of the

design, we changed the original parallel battery into a single cell. We moved the separator from the middle of the chamber to the top. This effectively simplified the assembly process of the robot. First, placing the battery to the top of the robot and using O-ring and bolt sealing avoids sealing the battery and Nafion with glue. In this way, anolyte and catholyte could be effectively isolated, and ion exchange could be performed through Nafion. Second, moving the battery up could avoid making holes in the center of the Nafion and electrodes, which ensured the integrity of the battery. To enable the unidirectional flow of electrolyte inside of the positive electrode so that the whole carbon felt can be saturated, two one-direction valves were added on the bottom plate of the battery.

During the battery test, since there were no obstacles or resistances between the cavity and the tentacles, the electrolyte would flow between these two chambers, and it was challenging to flow into the electrode through the one direction valve. Due to the lack of electrolyte infiltration, it was difficult to charge and discharge the battery. When the remaining electrolyte in the electrode has been consumed, there will not be enough reactant in the electrode to continue the charging process.

2.2.3 Third Generation

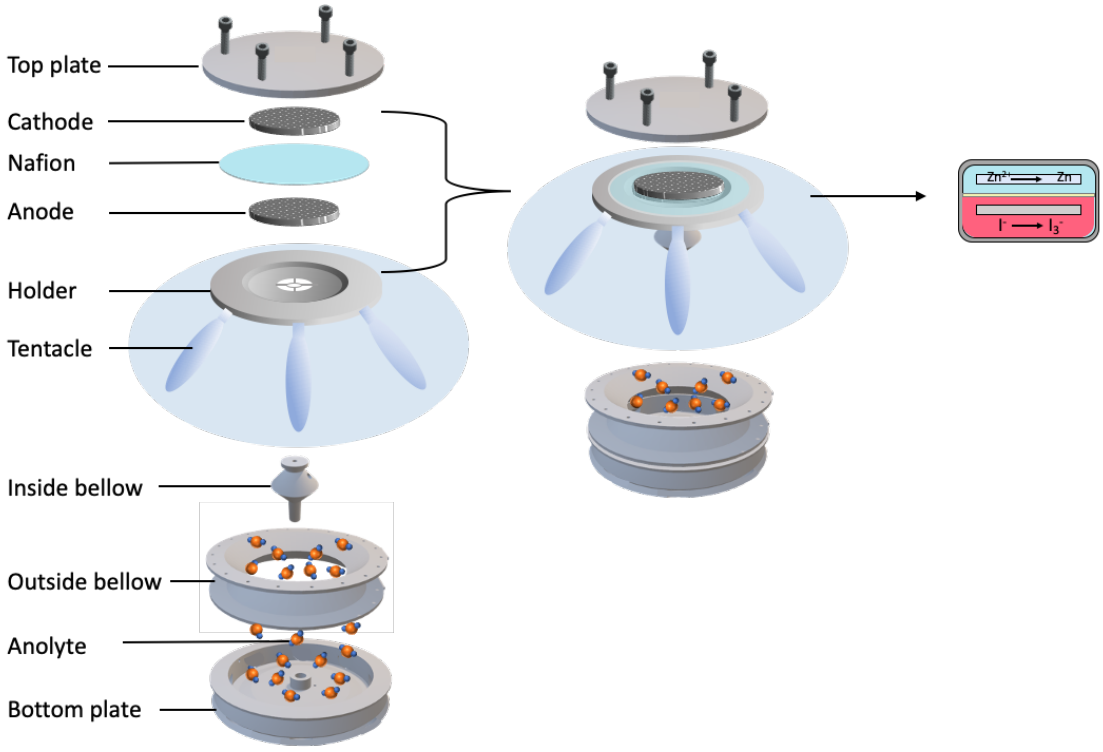

Figure 2.5 Assembly of the third generation jellyfish robot.

To achieve a continuous electrolyte flow between electrodes and tentacles (Figure 2.5), the tentacles were moved up to the top of the cavity, and leveled with the positive graphite felt. This ensured the electrolyte in the cavity could flow into the tentacles through the graphite felt after being squeezed. The flow battery's bottom plate was designed into a ring, with a central gap much larger than the valve in the second generation. This allowed the electrolyte to flow easily between the electrode and the cavity. Meanwhile, the stainless steel mesh was laser-cut into the same shape as the electrode, encapsulated close to the electrode. This could increase the contact area between the current collector and the graphite felt, and reduce the contact resistance compared with stainless steel wire. For the tentacles, it was hard to make Dragon Skin thin enough by molding. We then changed it to polyethylene, a polymer material. The plastic paper was cut into hexagonal structures

by laser, and the high temperature of the laser was utilized to stick the two pieces together to form a bag for electrolyte storage.

Different from the traditional flow battery design, in the design of the jellyfish robot, the pump was not needed to keep the electrolyte flow to accelerate the reaction speed. We improved the way to integrate the energy system in soft robot and used the ZnI_2 flow battery, not for actuation, but instead for controllable stiffening. Flow battery electrolyte worked as the tendon of the robot to make it swim. A flow battery powered the robot's motion, and at the same time, the robot's movement also promoted the discharging process of the flow battery.

2.3 Flow Battery Preparation

In the design of the ZnI_2 flow battery, we considered several factors affecting its performance. These factors include the electrode design, the current collector material, the ion conductive separator material, and the selection of the electrolyte solution.

First of all, it is required that the electrode does not participate in the redox reaction of the battery. Otherwise, the electrode material will no longer be stable after a few cycles of the cell, thereby reducing the battery performance. The reactions in the battery include the transfer of the reactants to the electrode surface, the transfer of the generated products to the solution, and the heterogeneous electron transfer of non-adsorbed substances. The speed of the electrode reaction is always determined by the slowest of the above three processes. By increasing the speed of the slowest step, the electrode's performance could be improved, thereby improving the performance of the battery system. As can be seen from Table 2.1, the carbon felt has a relatively high surface

area, but a lower resistance. Since the flow battery's performance is a function of the electrodes surface area, in our project, we chose the G100 graphite felt with a thickness of 3.2 mm and porosity of 0.83. It is less chemically reactive with high conductivities (both thermal and electrical).

Table 2.1 Properties of different graphic material electrodes.

Carbon materials	Carbon felt	Carbon cloth	Carbon paper
			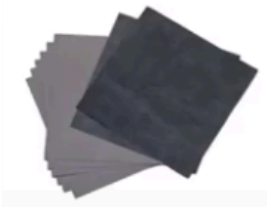
Thickness	3.2 mm	1 mm	0.4 mm
Advantage	High surface area; Can slightly bendable	High mechanical strength, bendable	High conductivity
Disadvantage	Relatively low conductivity	Low conductivity	Can't bend, easy to break

The function of the battery's current collector is to collect and transfer electrons produced during the reactions, so there should be a small ohmic resistance between the current collector and the electrode. The ZnI_2 solution is very corrosive; for example, the copper plate is easy to participate in the reaction process of the electrolyte because of corrosion. Therefore, the current collector must be corrosion resistant. Carbon plates and stainless steel are good choices. Since in our project, the current collector is required to be permeable for the electrolyte to flow through, we chose stainless steel 316 mesh with an open area of 31%, a hole of 30 um, and a thickness of 0.038 mm.

The ion-conducting membrane is also a vital battery component. The membrane materials can avoid the internal short circuit of the battery and selectively permeate the ions in the electrolyte. It can also prevent the active materials required for the positive and negative electrodes from mixing and avoid the concentration changes of the active materials participating in the reaction. For the separator of zinc iodine battery, we chose Nafion 115 in the present study to allow the Zn^{2+} and H_2O transfer. The Nafion 115 chosen has a conductivity of 0.1 min S/cm and a thickness of 127 μm.

2.4 Electrode Modification

When Nafion dries, its Teflon molecular chains contract together to prevent the conduction of ions. When Nafion absorbs water, its molecules are slowly dispersed by water molecules, creating a water channel, which provides conditions for the conduction of ions. The relationship between the ionic conductivity of the Nafion and water uptake follows the correlation below:

$$k = (0.005139\lambda - 0.00326)\exp\left[1268\left(\frac{1}{303} - \frac{1}{T}\right)\right] \quad \text{(Eqn 6)}$$

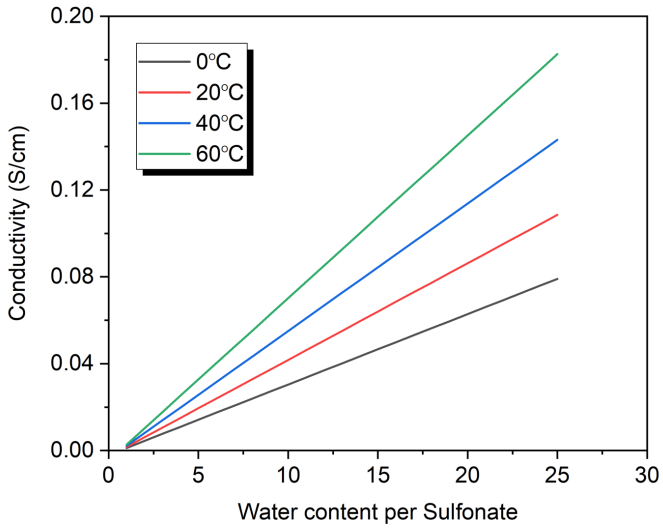

Figure 2.6 Conductivity of Nafion at different water content per Sulfonate.

As can be seen from Figure 2.6, both water content and temperature affect the ionic conductivity. The temperature can't be higher than 80°C, under which condition the Nafion will be inactivated. Typically, the ionic conductivity of the Nafion can reach 0.2 S/cm.

To clean the Nafion membrane and increase its ionic conductivity, we used 3 wt% H_2O_2, 0.5 M H_2SO_4, and 1 M $ZnCl_2$ to treat it. Below are the detailed steps:

1) The Nafion was immersed in the H_2O_2 solution to remove the dirt on it. It was kept at 60°C for 1 hour.
2) The Nafion was immersed into H_2SO_4 at 60°C for 1 hour. This process could store more protons into the Nafion.
3) The Nafion was immersed into $ZnCl_2$ at 60°C for 3 hours, and the pH of the solution was adjusted to 1 by HCl. Zn^{2+} would replace H^+ stored in the Nafion after the second step. Zn^{2+} stored inside of the Nafion would then help transmit Zn^{2+} from anolyte to catholyte at the beginning of the charging process.

After each step, the Nafion was washed by deionized (DI) water to remove the remaining solutions. Finally, it was stored in DI water before being assembling into the battery.

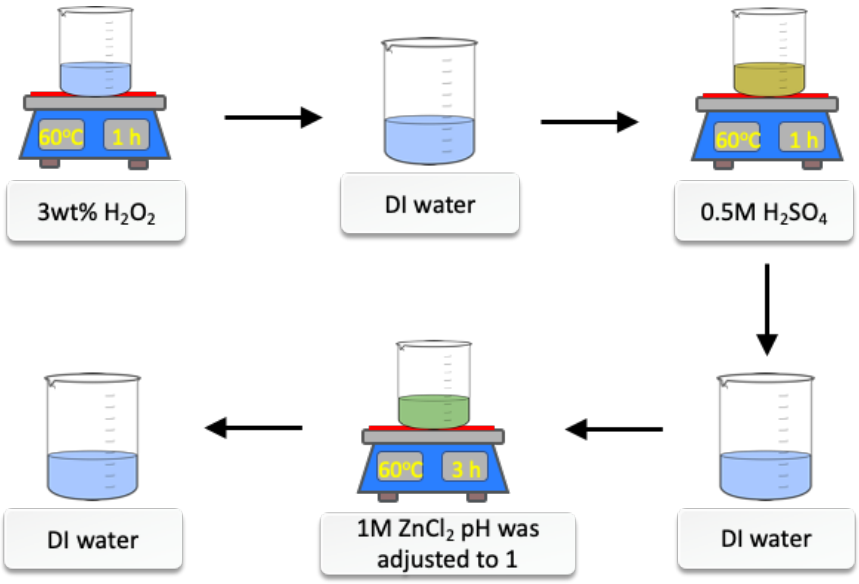

Figure 2.7 Schematic illustration of Nafion modification.

To improve the electrochemical property and hydrophilic of the graphite felt, it was pretreated by 95 wt% H_2SO_4. Below are the detailed steps:

1) The graphite felt was immersed into the H_2SO_4 at 50 °C for 4 hours.
2) It was washed by DI water to remove the remaining solutions.
3) It was heated at 60°C for 2 hours until dry.

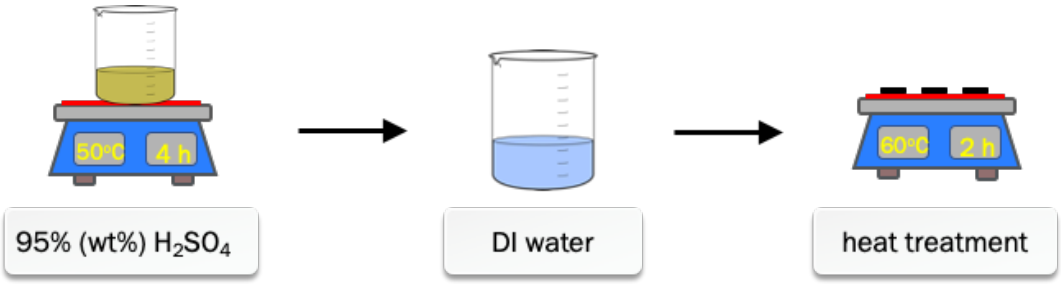

Figure 2.8 Schematic illustration of electrode modification.

The electrolyte with different concentrations was prepared by dissolving corresponding ZnI_2 (WGK Germany, ≥98%) into deionized water.

2.5 Electrochemical Characterization of Thin Film

In the thesis, the performance of the assembled ZnI_2 flow battery was tested using the BTS4000-5V6A battery testing system. Figure 2.9 shows the schematic diagram of the system. During the test, the red large crocodile clip and the small crocodile clip were both connected to the positive electrode of the battery. The black large crocodile clip and the small crocodile clip were clipped together to the negative electrode. The alligator clip was the current output electrode, and the small alligator clip was the voltage detection electrode. After checking the battery connections, we tested the battery performance according to the target programming parameters.

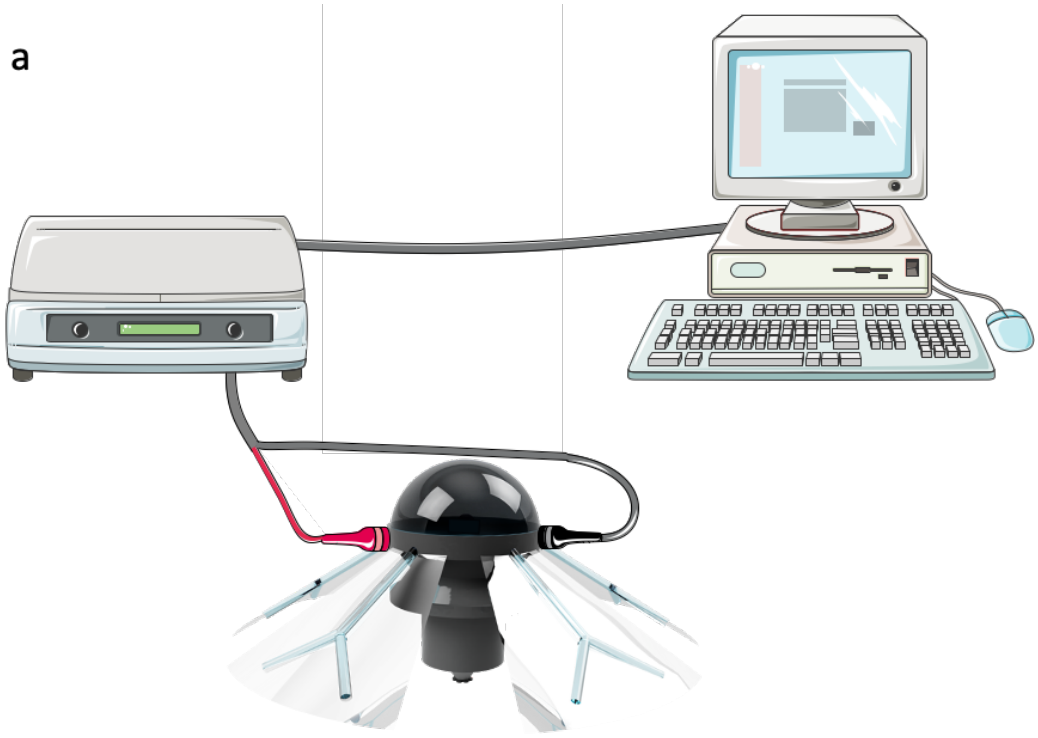

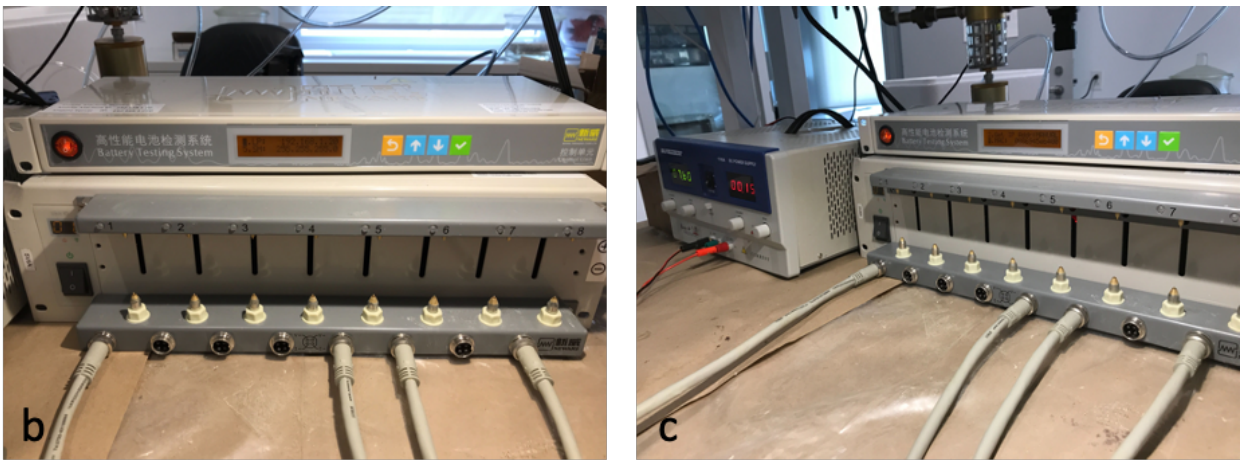

Figure 2.9 a) Schematic), b) and c) Photograph of the experimental set-up for the flow battery test.

3. Flow Battery Powered Jellyfish Robot: Experiment and Theoretical Evaluation

3.1 Introduction

Multi-functional energy storage can help create longer-operating robots. For soft robots, energy storage in the fluid form can be used for actuation, structure build-up, and other purposes. On the one hand, flow batteries can function as the power supply. On the other hand, the liquid components can also facilitate mechanical control. Here we improved the way to integrate the energy system in soft robots and allowed a different mechanical drive. To be specific, we made a demo of the jellyfish robot out of 3D printed parts and polymer films and adopted the ZnI_2 flow battery as the power supply system. In addition to providing the energy for the robot to swim, flow batteries also controlled the tentacle's stiffness for the jellyfish robot.

3.2 Materials and Methods

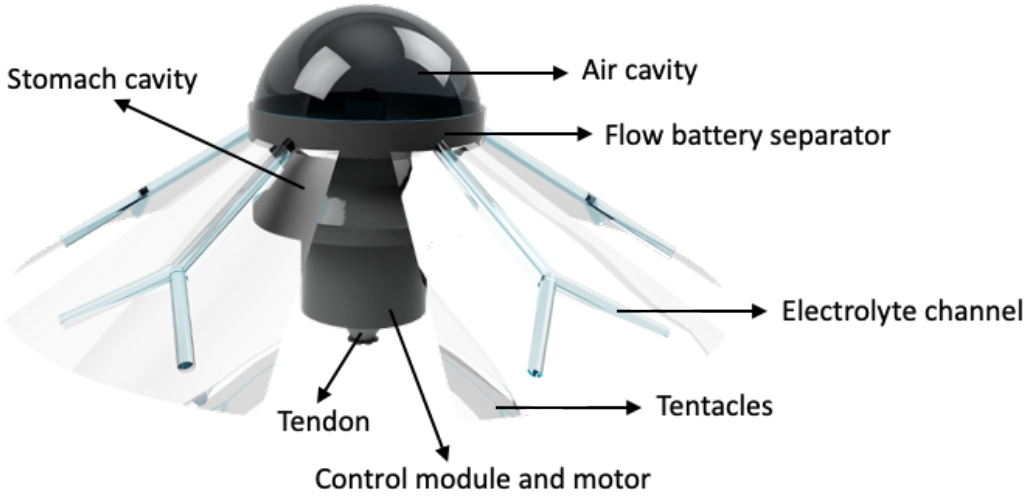

Figure 3.1 Structure of the jellyfish robot.

Figure 3.1 shows the schematic diagram of our jellyfish robot. We adopted the design of a half cell for the flow battery system. The electrolyte (ZnI_2) was stored in the stomach cavity and tentacles of the jellyfish, forming a circulating flow in between. When the flow battery was fully charged, it could provide all the external storage energy required for the operation of the jellyfish robot and the flow of electrolyte.

During charging, zinc was deposited on the negative electrode, while triiodide ions were produced in the solution at the positive side. During the swimming of the jellyfish robot when the battery was being discharged, the reverse process proceeded. The zinc ions acted as both charge carriers transported through the Nafion carrying water molecules and the reactant in the anolyte side of the battery.

The flow battery provided enough power to start the motor at the bottom of the jellyfish cavity. The motor was set to rotate in two directions. One end of the rope used as a tendon was fixed to the motor, while the other end was simultaneously attached to the top layer of the jellyfish, through the inside bellow. This bellow was adopted to isolate the tendon and the electrolyte in the cavity, providing sufficient support for the cavity to rebound.

The graphite felt for the flow battery cell was circular, with a diameter of 7 cm and a thickness of 3.2 mm. It was compressed by five bolts evenly distributed on the edge of the battery to 60% of its original thickness to reduce contact resistance. To prevent electrolyte leakage, Nafion was cut to the circular shape with a diameter of 7.5 cm. It was tightly sandwiched between two layers of graphite felt by the O-ring. Before charging, we injected electrolyte through the inlet and outlet

holes on the top of the battery to infiltrate the cathode graphite felt. After that, we sealed the inlet and outlet with sealing plugs. This ensured enough moisture for both sides of Nafion, and facilitated the exchange of ions in between. The total volume of anolyte was 26 mL, the same as the amount of liquid filling up all the tentacles of jellyfish. The electrolyte in the cavity of jellyfish was introduced with an injector and was kept sealed afterward.

During charging, we fixed the bottom of the jellyfish's battery and the tentacles and used a rotating device to push the top of the jellyfish. This ensured the continuous flow of anolyte, promoted the electrolyte uniformity, and accelerated the reaction rate.

3.3 Results and Discussion

As can be seen from Figure 3.2, before charging, the electrolyte was light yellow. As the charging progressed, the electrolyte turned to dark yellow, light red, and finally dark red. This change was because the reaction of I^- in the electrolyte generated iodine during the charging process. At the same time, zinc was formed on the negative graphite felt. During discharging, the color of the electrolyte changed in the opposite direction, from dark red to light yellow.

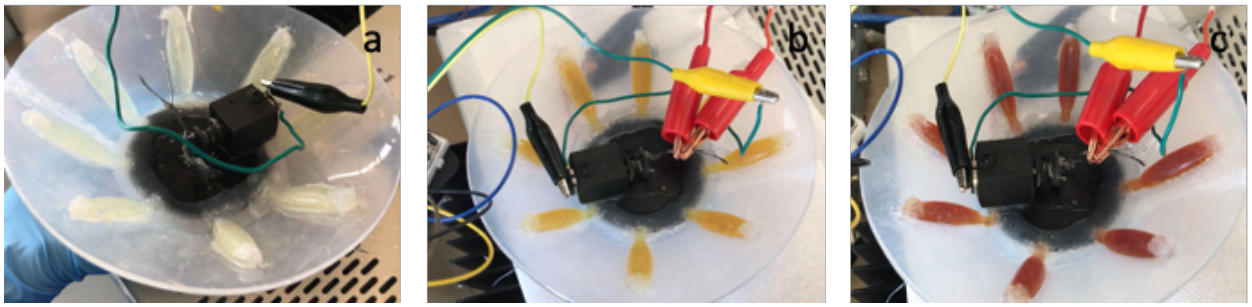

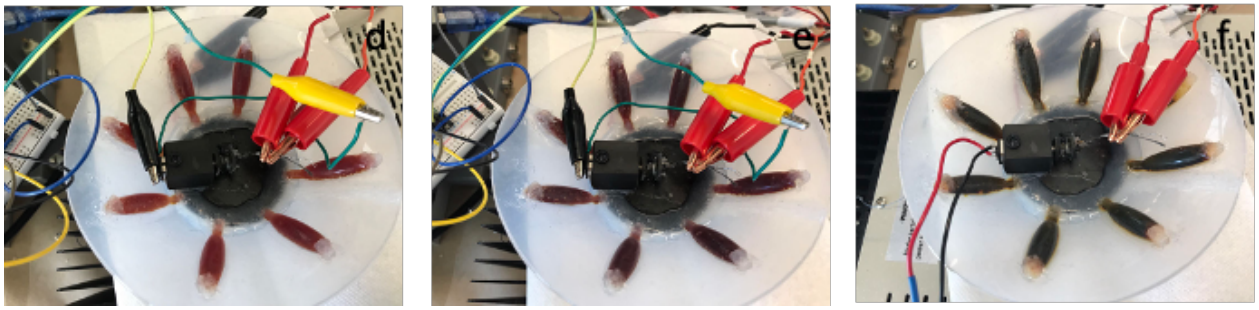

Figure 3.2 Color change of electrolyte during the flow battery's charging process.

When the flow battery was discharged, the output voltage was about 1.3 V. This voltage powered the motor at the bottom of jellyfish. Meanwhile, the electrolyte flow inside of the jellyfish worked as the tendon and provided controllable stiffness to help the robot swim. As the motor rotated in one direction, the tendon was rolled. The tension caused by the reduction in the tendon length compressed the cavity where the electrolyte was stored. The electrolyte was squeezed into the jellyfish tentacles from the cavity. When the electrolyte filled the tentacles made of plastic paper, the stiffness of the tentacles increased, and another motor of the flow battery pulled the top of the tentacles to gather. Since the stiffness for the tentacles was enough, it then swang down the water while gathering. This provided enough thrust for the upstream movement of jellyfish. When the motor rotated in the reverse direction, the tendon was released. Then the cavity returned to its original shape due to the rebound of the bellow. Simultaneously, the electrolyte flowed back into the cavity from the tentacle, and the tentacles made of thin plastic paper turned soft. This made the tentacles open without resistance, which would stop the jellyfish from returning to its original position.

It has been found that a high concentration of the electrolyte favors energy output in the flow battery. To understand its effect on the battery's capacity, we tested the battery performances under three concentration levels for the electrolyte: 1.5 M, 3 M, and 5 M at the current density of 5

mA/cm^2. Throughout the experiments, we maintained the system at ambient temperature, a constant flow rate of 80 mL/min, and a fixed overall electrolyte volume of 26 mL. Figure 3.3 below shows the effect of electrolyte concentration on the capacity of the flow battery. As the electrolyte concentration rose from 1.5 M to 5 M, the battery capacity increased from 22 Ah/L to 66 Ah/L due to the presence of more active materials. The energy efficiency, however, saw a ~20% decrease as the concentration changed from 1.5 M to 5 M, due to the increasing electrolyte resistance.

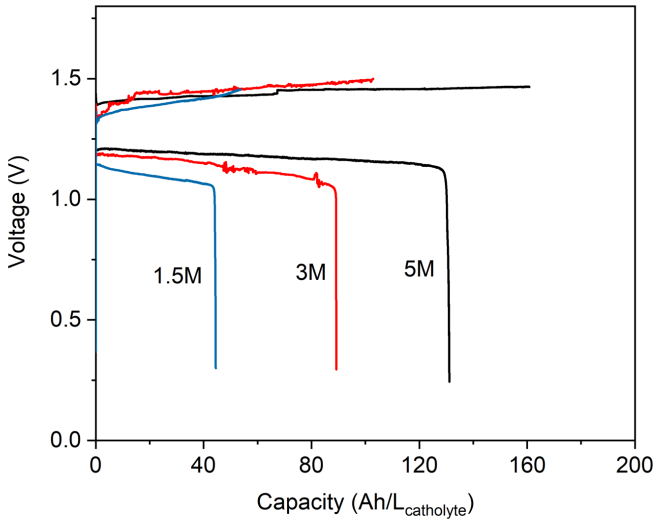

Figure 3.3 Charge/discharge curves for the flow battery with 1.5 M, 3 M, and 5.0 M ZnI_2 at the current density of 5 mA/cm^2.

3.3.1 Theoretical Evaluation of Maximum Swimming Duration

Since the diameter of the graphite felt electrode is 7 cm, the area of the electrode graphite felt is calculated to be $\pi \times (7/2 \text{ cm})^2 = 38.48 \text{ cm}^2$. The saturation concentration of the electrolyte is 5.6 M [51], and the volume is 26 mL. As mentioned in Chapter 2, the capacity of the ZnI_2 flow battery is 111.96 mAh/g. Therefore, the total energy in the battery is calculated to be 0.026 L × 322 Wh/L = 8.372 Wh.

Through experiments, we have also validated that it takes about 0.5 Watts to power all the electric modules in the robot. Based on the calculations above, the theoretical evaluation of the maximum swimming duration of the jellyfish robot should be 8.372 Wh/0.5 W = 16.74 h.

3.3.2 Comparison of Different Energy Supply Systems

To demonstrate the advantages of the flow batteries, we compare the energy cost of transport (COT) of the robot powered with and without a flow battery (i.e., powered by lithium-ion battery). COT quantifies the energy efficiency of transporting an object from one place to another. It is defined as

$$COT = \frac{E}{mgd} \quad \text{(Eqn 7)}$$

where E is the energy input to the system, m is the mass of the robot, d is the moving distance in total, and g is standard gravity.

For the swimming robot, the index of the mass should be 0.4. To simplify the comparison, we set the swimming distance as a constant, which means the demos need the same amount of energy to power all the swimming process. Meanwhile, a boost module was used for balancing the current and voltage to keep the power output of the flow battery and solid battery at the same level. In the jellyfish robot powered by a lithium-ion battery, to keep the same design and driven mechanism of the robot, the electrolyte was changed to water as an alternative to control the stiffness of the tentacles. Here, we assumed water had the same density as that of the electrolyte. Besides, the cavity for air to provide the buoyancy was designed to be larger, to overcome the gravity increase

of the robot when powered by a solid battery. The lithium-ion battery has an energy output of 4.44 Wh and a weight of 22 g. As calculated before, the total energy that can be provided by the flow battery in the jellyfish robot is 6.72 Wh. Thus, to achieve the same energy capacity as the flow battery system, the number of lithium-ion batteries needed is calculated as 6.72 Wh/4.44 Wh = 1.5, which brings an additional weight of 1.5 × 22 g = 33 g to the system. The fractional increase in energy efficiency can be simplified as:

$$\text{Fractional increase} = \frac{m^{0.4}{}_{solid\ battery\ system}}{m^{0.4}{}_{flow\ battery\ system}} - 1 \qquad \text{(Eqn 8)}$$

Since the weight of the robot powered by flow battery is 100g, the adoption of solid batteries will bring the wight of the system to 1.5 × 22 g + 100 g = 133 g. Compared with the solid battery-based system, the fractional increase in energy efficiency for the flow battery-based system is (133 g – 100 g)$^{0.4}$/100 g = 12.1%.

Based on the analysis above, we can readily conclude that the adoption of flow batteries in the jellyfish robot has threefold advantages compared with traditional systems powered by solid batteries. First, it decreases the overall weight of the robotic system by getting rid of solid batteries. Second, it simplifies the design by integrating different functions (e.g., actuation or structure) in the energy storage system. Third, it increases the system's overall energy efficiency.

4. Graphite Felt Electrode Compression

4.1 Introduction

The porous electrode is a critical component that determines the overall performance of the battery, where electrochemical reactions occur, and the conversion of electrical energy and chemical energy is realized. The conductivity, stability, and electrochemical activity of the electrode materials directly affect the energy density, macroscopic charge, discharge performance, and life cycle of the battery. The multi-component, multi-scale, and multi-form thermal and mass transport processes (convection, diffusion, migration) in the electrode are affected by the property and microstructure of the electrode materials. The active substance in the electrolyte accepts or releases electrons on the electrode surface to perform an electrochemical reaction. This realizes the transformation between electrical energy and chemical energy, completing the storage or release of energy. The ideal electrode should exhibit excellent reactivity, toughness, stability, electrical conductivity, mechanical strength, and a high specific surface area. At the same time, the electrode materials should be low in cost and readily available.

Researchers at the University of New South Wales in Australia first used lead (Pb), gold (Au), platinum (Pt), titanium-based platinum (Pt-Ti), and titanium-based iridium oxide as the flow battery electrode materials[80, 81]. They have shown that in addition to high cost, Au has poor electrochemical reversibility. Pb is also costly with weak electrochemical reversibility and is easy to form a high-resistance passivation film on the electrode surface, thus inhibiting the reaction. The cost of titanium-based platinum and titanium-based iridium oxide is also high; therefore, they not suitable for large-scale applications. Wang *et al.* found that graphite-based materials, such as graphite felt, graphite paper, etc., exhibited better connectivity, high specific surface area, high

electrical conductivity, with reasonable stability. These qualities make them suitable as electrode material for use in flow batteries[62]. In the porous graphite felt fiber electrode, fibers overlap and interweave to form a complex three-dimensional pore network structure, which provides a circulation path for the transport of strong acid electrolytes. Electrode materials should offer reactive sites for electrochemical reactions, achieving material conversion and electron conduction, and graphite felt proves to be an excellent electrode material for its proper porosity, high reactivity, reversibility, and corrosion resistance[82]. In flow batteries, graphite felt could be divided into two types: rayon and polyacrylonitrile (PAN) based on the fiber materials. Zhong *et al.* compared the two electrode materials and found that PAN-based graphite felt had good conductivity, and the fiber crystallites were tiny[83]. The surface of the fiber had more unsaturated graphite atoms, thus enhancing the electrochemical activity for vanadium ions on the surface of the PAN-based graphite felt. However, if untreated and used directly in the flow battery electrodes, graphite fibers can be easily oxidized and will fall off during long-term use. Therefore, it is necessary to properly modify the graphite felt to improve its electrochemical reactivity, reversibility and hydrophilicity, and reduce the polarization overpotential of this electrode material.

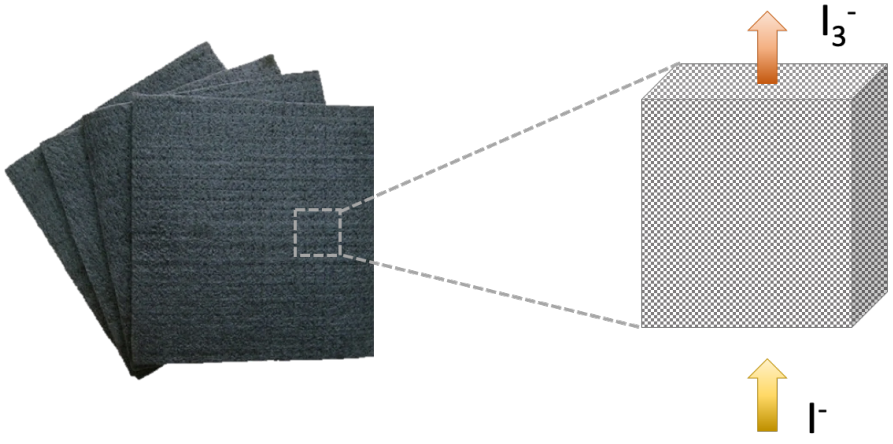

Figure 4.1 Schematic diagram of graphite felt electrode and its internal electrolyte transport.

We have modified the graphite felt with sulfuric acid to improve its electrochemical property, as described in Chapter 2.4. The surface of the porous graphite felt electrode is rough. In the absence of external forces, the contact area between the graphite felt electrode and the current collector plate is small, which will produce a considerable contact resistance. This will increase the internal resistance of the battery and reduce its performance in charging and discharging. A pressing force needs to be applied during the battery assembly process to improve the contact between the electrode and the current collector plate, thereby reducing the contact resistance. Under pressing force during battery assembly, the pore structure of the porous electrode material will change significantly. The electrolyte transport and electrochemical reaction speed inside the electrode will also be affected.

4.2 Materials and Methods

For flow batteries with different structures, the electrode compression deformation exhibits different morphological characteristics. Figure 4.2 shows the schematics of the electrode compression deformation for flow batteries. The fixture mainly consisted of endplates, copper sheets, O-ring, and bolts. The cavity of the RPU endplate was 3 cm in diameter. The depth of the cavity equals the thickness of the graphite felt and copper sheet. In the assembly process of a battery without flow channels, the electrode is uniformly compressed to the cavity by endplates. The degree of the compression was adjusted by tuning the depth of the endplate cavity. To accurately measure the resistance change of graphite felt electrode materials during compression, a piece of copper sheet was attached to the felt at each side with a small piece sticking out for Ohm connection. After that, the testing system was sealed tightly with bolts and O-rings. In general, the corrosion-resistant insulating O-ring plays a vital role in sealing the electrolyte.

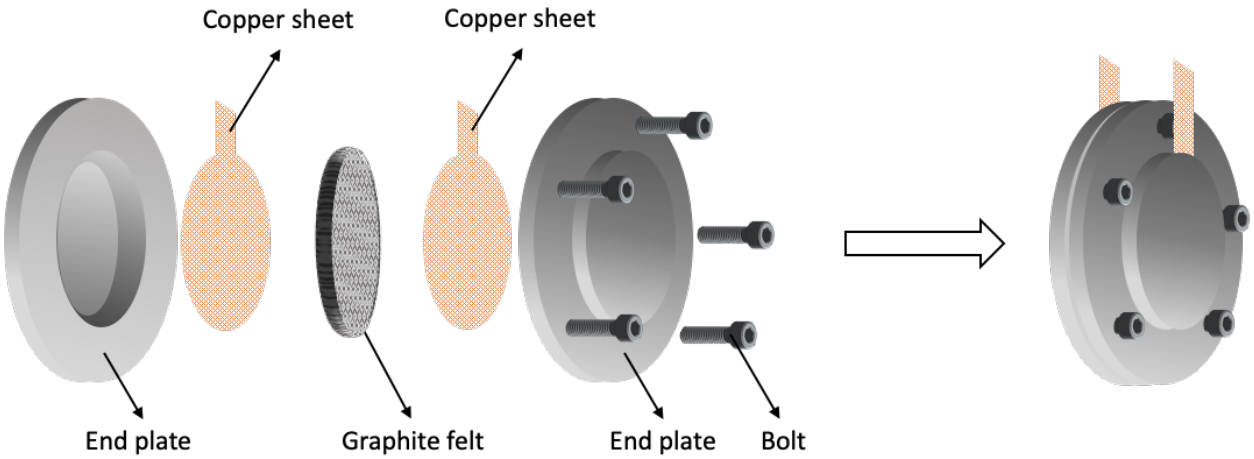

Figure 4.2 Schematic diagram for the electrode compression test.

The initial thickness of the graphite felt is 3.2 mm, and is defined as h_0. The electrode thickness after compression is denoted as h_e. Then the compression ratio (CR) is calculated as:

$$\mathrm{CR} = \left(1 - \frac{h_e}{h_0}\right) \times 100\% \qquad \text{(Eqn 9)}$$

Based on the equation, if we want to achieve electrode compression ratios at 0%, 20%, 40%, 60%, the corresponding effective thicknesses of the graphite felt are 3.2 mm, 2.56 mm, 1.92 mm, and 1.28 mm, respectively.

4.3 Results and Discussion

4.3.1 Effect of Compression Ratios on Porosity

Compression changes the geometry of the electrode material, resulting in reduced electrode thickness and porosity. Porosity is the main parameter that affects the fluid flow characteristics of porous media. For porous electrode materials, porosity affects the flow state of the electrolyte and

the distribution of reactants, which in turn affects the energy efficiency of the battery. Therefore, by calculating the changes in electrode porosity at different electrode compression ratios, we can reveal the effect of electrode compression on electrolyte transport.

The porosity of the graphite felt electrode that is uniformly compressed can be calculated according to CR and the initial porosity (ε_0) of the electrode material[84-86]:

$$\varepsilon = \frac{\varepsilon_0 - CR}{1 - CR} \quad \text{(Eqn 10)}$$

Here, the graphite felt has an initial porosity of 0.83, and constructed electrode structures have compression ratios of 0%, 20%, 40%, and 60%. During calculation, it is assumed that only the internal pores of the electrode are compressed, the solid fibers are not damaged or overlapped during compression. Fiber diameter, as well as the number of fibers, also remains unchanged. According to Eqn 10, the compression ratios at 0%, 20%, 40%, and 60% correspond to porosity levels at 0.83, 0.79, 0.72, and 0.58, respectively. Figure 4.3 shows the reconstruction geometries for uncompressed and compressed electrodes, with compression ratios ranging from 0% to 60%.

Porosity is always inversely proportional to the compression strain[62]. When the electrode compression ratio exceeds 40%, porosity exhibits an evident decrease. In this case, the associated assembly time and cost will increase dramatically as the compression ratio continues its rising trend.

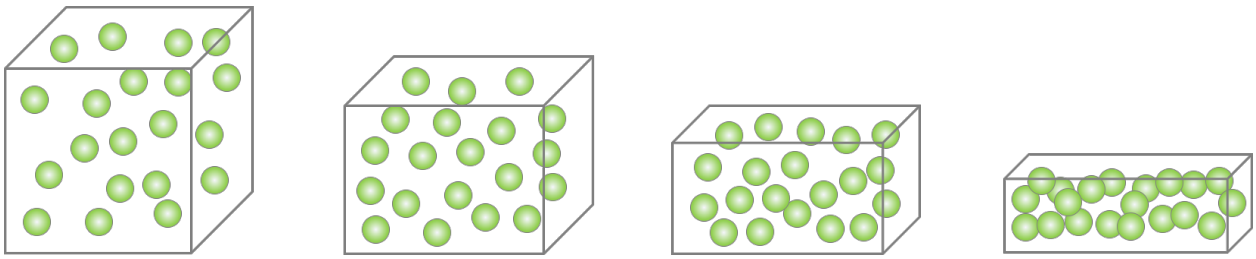

Figure 4.3 Reconstruction of electrodes at different compression ratios.

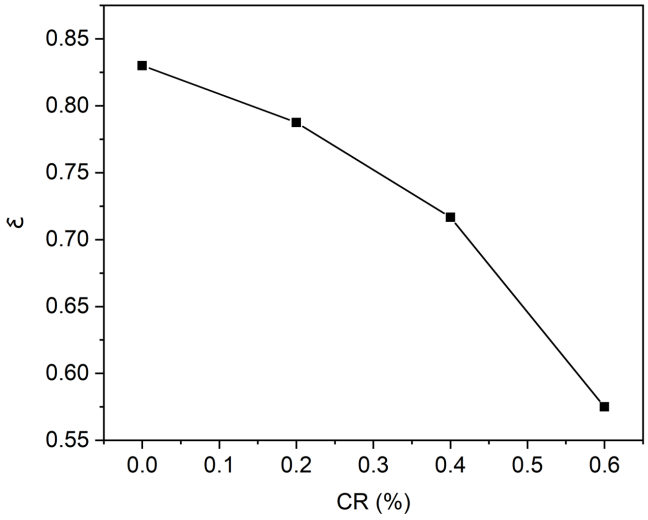

Figure 4.4 Electrode porosity at different compression ratios.

4.3.2 Effect of Compression Ratios on Resistance

In a flow battery, when the graphite felt electrode material is being compressed, the contact area between the electrode and the current collector will increase. This can effectively reduce the contact resistance in between. Moreover, the internal pores of the compressed electrode material decrease, increasing the contact area between graphite fibers. During the test, a small voltage is applied through the copper sheet to detect the current value in the loop; then, the total resistance is calculated according to Ohm's law. The electrode resistance is then calculated by subtracting the copper sheet's resistance from the total.

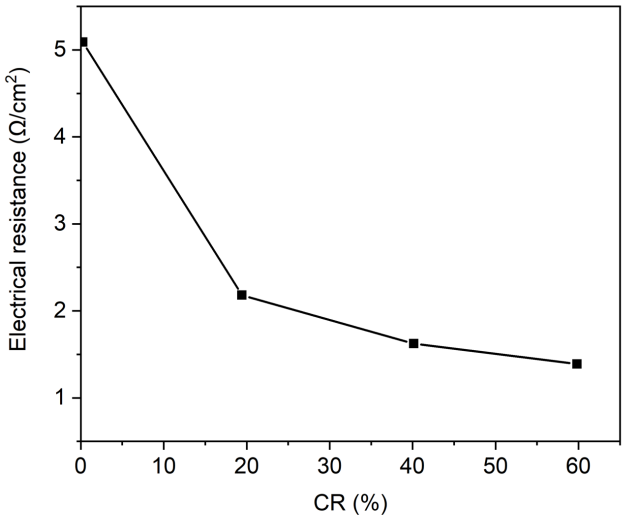

Figure 4.5 Electrode electrical resistance at different compression ratios.

4.3.3 Effect of Compression Ratios on Battery Performance

It has been found that the compression favors the conductivity of graphite felt and also the close contact between the electrode and current collector. To understand the effect of compression on the flow battery performance, we tested the charging/discharging performances under four electrode compression ratios: 0, 20%, 40%, and 60%. The volume of the electrolyte is 30 ml, and the concentration is 3 M. Throughout the experiments, we maintained the flow rate of the electrolyte at 80 mL/min, and a fixed current density of 5 mA/cm^2. Figure 4.6 a below shows the charging and discharging process of the flow battery at different electrode compression ratios. With the increase of compression ratios, the corresponding working time of the flow battery increased from 2 h to nearly 4 h. This is because the contact resistance decreased when we compress the carbon felt. It helps the transfer of electrons inside the battery and more energy lost beacause of Ohmi lose will be saved. Figure 4.6 b shows the energy efficiency of the batteries. Although the compression ratio of 60% has a lower contact resistance, its battery's energy

efficiency was lower than that of the compression ratio of 40%. The increase in charge and discharge time gradually becomes a factor that inhibits the increase in energy efficiency. As the charge and discharge time gradually increases, the net convective crossover of anolyte and catholyte increases and decays the battery capacity, resulting in a decrease in energy efficiency.

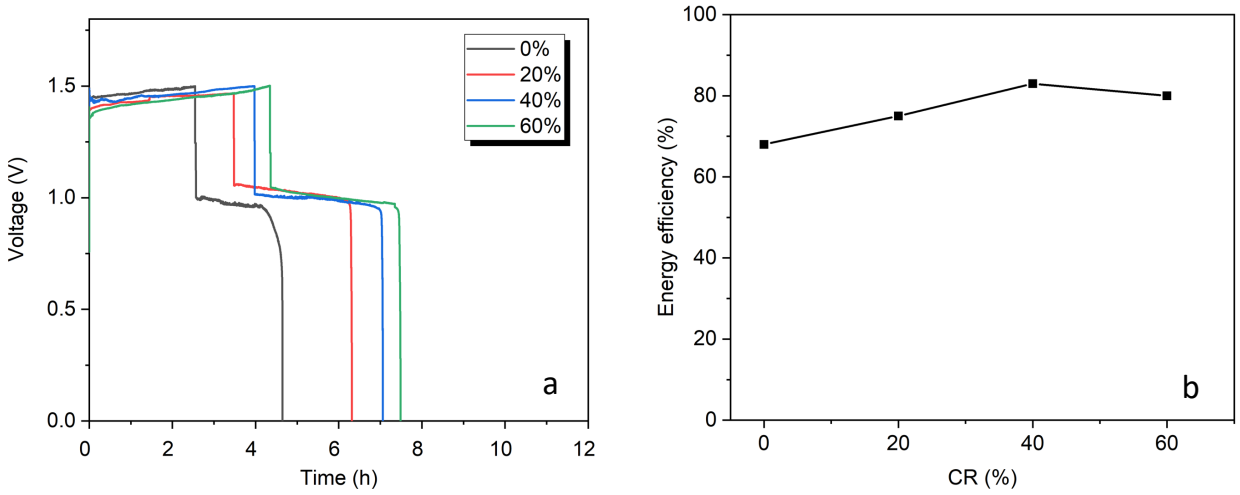

Figure 4.6 (a) Charge/discharge curves and (b) energy efficiency for the flow battery at different electrode compression ratios.

5. Dendrite: Mechanism and Inhibition Method

5.1 Introduction

When zinc ions are electron-deposited on the negative electrode to form metallic zinc, the crystalline form of zinc will be deicded by the overpotential between the electrode and electrolyte. When the concentration of zinc ions is high and the deposition current is low, leading to a low concentration overpotential. In this case, it is easy to form zinc like flowers or pebbles. Under high current densities, the reaction rate of Zn^{2+} is too fast, so that the reactant cannot be transferred to the electrode surface in time for reaction. Afterward, the low concentration of zinc ion and a high concentration overpotential is produced on the electrode surface; then, Zn dendrite crystals are likely to form. Three main factors affect the growth of dendrites: the electrochemical polarization of the electrode process, the material transfer conditions of the reactants, and the type and content of surface-active substances in the solution. When the electrochemical overpotential is low, the growth of the crystals is relatively uniform, and dendrites are hard to form. In this case, concentration polarization is small, and the mass transfer is facilitated. In the later period of charging, the concentration of zinc ions decreases as the overpotential rises. This causes a large concentration polarization, so the dendrite growth is more significant.

The formation mechanism of zinc dendrites has been studied for many years. Researchers generally believe that the charging process is mainly controlled by the mass transfer process of the liquid phase. During charging, the concentration of the reactive ions close to electrode is relatively low, and the concentration overpotential is high. It is easier for the reactant ions to deposite on the tips of the zinc layer than to other locations. Therefore, the zinc deposition rate is higher at the surface protrusions, resulting in the formation of zinc dendrites. Especially, as zinc

electrodeposition is performed at a high current density, the transfer rate of ions in the solution is less than the reaction rate of the electrode surface. The reactant ions in the solution near the electrode surface become very scarce, causing a large concentration overpotential. The reactant ions in the solution are easier to diffuse to the protrusions, thus forming zinc dendrites.

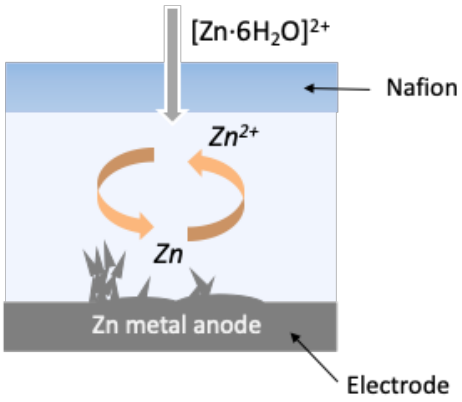

Figure 5.1 The forming processes of zinc dendrites.

During charging, as the reaction progresses, zinc dendrites that are continuously deposited and grown on the electrode surface will penetrate the Nafion and cause a short circuit between the electrodes. This causes the battery cycle life to decrease and the thickness of the zinc layer to vary after a long time of charging. Under this condition, the battery cannot be discharged continuously, resulting in a decrease in energy efficiency. The growth of dendrite crystals includes two processes: nucleation and crystal growth. Low current densities and high flow rates help prohibit the formation of Zn dendrites. But a smaller current will inevitably increase the charging time. The moving frequency of the tentacles also limits the flow rate of the battery in the jellyfish robot. Apart from that, methods for inhibiting zinc dendrites are generally divided into the following three types. The first method is to use electrode additives, usually metal or metal oxides, such as Pb, Cd, In, etc., to improve the conductivity of the electrode materials. This makes Zn^{2+} easy to transfer in the solution so they can be evenly deposited on the electrode surface, and the protrusions

on the electrode surface are reduced. Since the possible growth sites of zinc dendrites (i.e., protrusions) are reduced, the growth of zinc dendrites is inhibited. The second method is to improve the membrane performance of the flow battery. By controlling the pore size, porosity, and thickness of the membrane material, the growth of dendrites can be controlled. The ion passing rate, the blocking rate of zincate ions, and the internal resistance of the membrane are critical criteria during selection. The third method is to add additives to the electrolyte. Common additives include metal ions and organic additives. Metal ions can act as electrode additives to reduce the growth of zinc dendrites. Organic additives (e.g., alcohol, etc.) can also enable uniform deposition of zinc on the electrode surface to inhibit dendrite growth, thus avoiding short circuits inside the energy storage device. Our project used ethanol as an organic additive to study the performance changes of flow batteries.

5.2 Materials and Methods

To examine the prohibitory effect of ethanol on Zn dendrite formation, we tested the flow battery systems with and without ethanol additives to the electrode surface. The concentration of the ZnI_2 electrolyte was 3 M. The charge and discharge current density was fixed at 5 mA/cm^2.

5.3 Results and Discussion

Figure 5.2 shows that adding ethanol to the electrolyte helps inhibit the growth of zinc dendrites. When no alcohol was added, uneven Zn deposition occurred on the electrode surface after charging. The dendrite broke the Nafion and stopped the battery's discharge process. After the flow battery with added ethanol additives was charged, Zn would be densely deposited on the surface of the electrode. This resulted from the ethanol's coordination with the zinc ions. Ethanol complexed

with zinc ions and improved the mass transfer in the electrolyte. This would decrease the concentration overpotential close to the electrodes and make the zinc surface smoother.

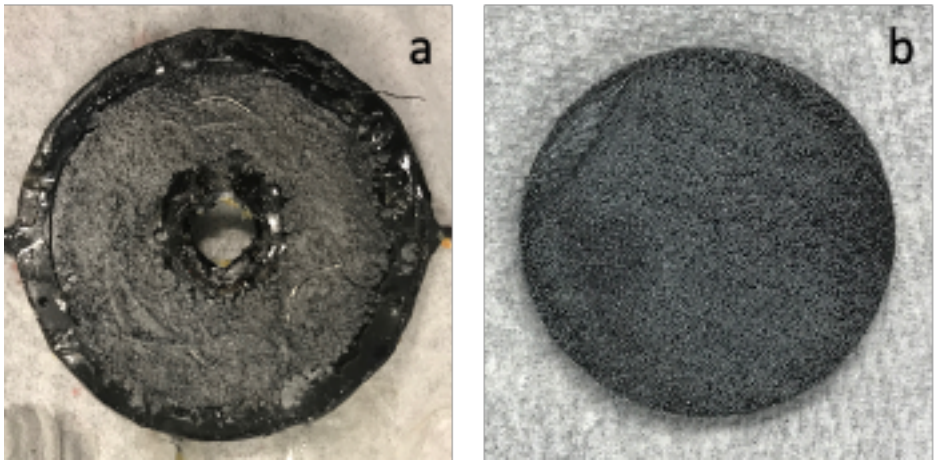

Figure 5.2 Morphologies of zinc dendrites after charging (a) without EtOH and (b) with 10% EtOH in the electrolyte.

6. Summary and Future Work

Soft robots resemble living creatures in their flexibility to move and adapt. In this thesis, we have designed a flexible jellyfish robot. The motor rotation drives the tentacles movement and enables the robot to swim. The key innovation presented in this work is to replace traditional "rigid" secondary batteries with "soft" flow batteries, which are used as the power supplies for the jellyfish robot system. Chapter 1 introduces the field of soft robotics and identifies the research gap in designing "soft" power systems. Chapter 2 describes the design iterations for the flow battery system, followed by electrode modification and some electrochemical characterizations. Chapter 3 is centered around the swim test for the jellyfish robot, and comparatively evaluates the flow battery-based systems with other traditional energy systems. Chapter 4 studies the effect of electrode compression ratios on the electric resistance and the permeability for the battery system. Chapter 5 introduces the principles of dendrite formation and investigates the optimal amount for ethanol additive to the electrolyte.

The following conclusions can be drawn from the present work:

1) A ZnI_2 flow battery based jellyfish robot system is successfully designed and optimized.

2) The maximum swimming time with the current flow battery system could reach 16.74 h.

3) In addition to being soft, the flow battery system exhibited comparable advantages over traditional energy systems. Compared with the system powered by a lithium battery, the fractional increase in energy efficiency in the flow battery system is 12.1%.

4) The effect of compression ratios of the electrode material on electric resistance and permeability was studied.

5) Through the addition of ethanol, dendrites generated during the charging of the flow battery can be effectively avoided. The inhibitory effect of ethanol on dendrite growth was examined experimentally.

Future work includes:

1) Explore pathways to improve the electrochemical performance (e.g., energy density) for the flow battery system as described.

2) Integrate the flow battery into the jellyfish robot to conduct an experimental evaluation of the maximum swimming duration.

References

1. Zuckerman, O.; Walker, D.; Grishko, A.; Moran, T.; Levy, C.; Lisak, B.; Wald, I. Y.; Erel, H. In *Companionship Is Not a Function: The Effect of a Novel Robotic Object on Healthy Older Adults' Feelings of" Being-Seen"*, Proceedings of the 2020 CHI Conference on Human Factors in Computing Systems, 2020; pp 1-14.

2. Hu, Y.; Hoffman, G. In *Using skin texture change to design emotion expression in social robots*, 2019 14th ACM/IEEE International Conference on Human-Robot Interaction (HRI), IEEE: 2019; pp 2-10.

3. Huang, C.-M.; Mutlu, B. In *Anticipatory robot control for efficient human-robot collaboration*, 2016 11th ACM/IEEE international conference on human-robot interaction (HRI), IEEE: 2016; pp 83-90.

4. Nikolaidis, S.; Zhu, Y. X.; Hsu, D.; Srinivasa, S. In *Human-robot mutual adaptation in shared autonomy*, 2017 12th ACM/IEEE International Conference on Human-Robot Interaction (HRI, IEEE: 2017; pp 294-302.

5. Hoffman, G.; Vanunu, K. In *Effects of robotic companionship on music enjoyment and agent perception*, 2013 8th ACM/IEEE International Conference on Human-Robot Interaction (HRI), IEEE: 2013; pp 317-324.

6. Liu, G.; Li, T.; Peng, Y.; Hou, X. In *The ant algorithm for solving robot path planning problem*, Third International Conference on Information Technology and Applications (ICITA'05), IEEE: 2005; pp 25-27.

7. Wu, T.-M., The inverse kinematics problem of spatial 4P3R robot manipulator by the Homotopy Continuation Method with an adjustable auxiliary Homotopy function. *Nonlinear Analysis: Theory, Methods & Applications* **2006,** *64* (10), 2373-2380.

8. Yang, X.; He, K.; Guo, M.; Zhang, B. In *An intelligent predictive control approach to path tracking problem of autonomous mobile robot*, SMC'98 Conference Proceedings. 1998 IEEE International Conference on Systems, Man, and Cybernetics (Cat. No. 98CH36218), IEEE: 1998; pp 3301-3306.

9. Wagner, C. R.; Howe, R. D., Force feedback benefit depends on experience in multiple degree of freedom robotic surgery task. *IEEE Transactions on Robotics* **2007,** *23* (6), 1235-1240.

10. Hillel, A. T.; Kapoor, A.; Simaan, N.; Taylor, R. H.; Flint, P., Applications of robotics for laryngeal surgery. *Otolaryngologic Clinics of North America* **2008,** *41* (4), 781-791.

11. Balasubramanian, R.; Dollar, A. M., Performance of serial underactuated mechanisms: Number of degrees of freedom and actuators. In *Redundancy in Robot Manipulators and Multi-Robot Systems*, Springer: 2013; pp 1-13.

12. Silverthorn, D. U.; Ober, W. C.; Garrison, C. W.; Silverthorn, A. C.; Johnson, B. R., *Human physiology: an integrated approach*. Pearson/Benjamin Cummings San Francisco: 2010.

13. Kim, S.; Laschi, C.; Trimmer, B., Soft robotics: a bioinspired evolution in robotics. *Trends in biotechnology* **2013,** *31* (5), 287-294.

14. Purcell, E. M., Life at low Reynolds number. *American journal of physics* **1977,** *45* (1), 3-11.

15. Huang, C.; Lv, J.-a.; Tian, X.; Wang, Y.; Yu, Y.; Liu, J., Miniaturized swimming soft robot with complex movement actuated and controlled by remote light signals. *Scientific reports* **2015,** *5* (1), 1-8.

16. Bartlett, N. W.; Tolley, M. T.; Overvelde, J. T.; Weaver, J. C.; Mosadegh, B.; Bertoldi, K.; Whitesides, G. M.; Wood, R. J., A 3D-printed, functionally graded soft robot powered by combustion. *Science* **2015,** *349* (6244), 161-165.

17. Wehner, M.; Truby, R. L.; Fitzgerald, D. J.; Mosadegh, B.; Whitesides, G. M.; Lewis, J. A.; Wood, R. J., An integrated design and fabrication strategy for entirely soft, autonomous robots. *Nature* **2016,** *536* (7617), 451-455.

18. Shepherd, R. F.; Ilievski, F.; Choi, W.; Morin, S. A.; Stokes, A. A.; Mazzeo, A. D.; Chen, X.; Wang, M.; Whitesides, G. M., Multigait soft robot. *Proceedings of the national academy of sciences* **2011,** *108* (51), 20400-20403.

19. Duduta, M.; Clarke, D. R.; Wood, R. J. In *A high speed soft robot based on dielectric elastomer actuators*, 2017 IEEE International Conference on Robotics and Automation (ICRA), IEEE: 2017; pp 4346-4351.

20. Xu, L.; Chen, H.-Q.; Zou, J.; Dong, W.-T.; Gu, G.-Y.; Zhu, L.-M.; Zhu, X.-Y., Bio-inspired annelid robot: a dielectric elastomer actuated soft robot. *Bioinspiration & biomimetics* **2017,** *12* (2), 025003.

21. Li, W.-B.; Zhang, W.-M.; Zou, H.-X.; Peng, Z.-K.; Meng, G., A fast rolling soft robot driven by dielectric elastomer. *IEEE/ASME Transactions on Mechatronics* **2018,** *23* (4), 1630-1640.

22. Niu, S.; Luo, Y.; Shen, Y.; Kim, K. J. In *Enabling earthworm-like soft robot development using bioinspired IPMC-scissor lift actuation structures: Design, locomotion simulation and experimental validation*, 2015 IEEE International Conference on Robotics and Biomimetics (ROBIO), IEEE: 2015; pp 499-504.

23. Huang, X.; Kumar, K.; Jawed, M. K.; Nasab, A. M.; Ye, Z.; Shan, W.; Majidi, C., Chasing biomimetic locomotion speeds: Creating untethered soft robots with shape memory alloy actuators. *Science Robotics* **2018,** *3* (25), eaau7557.

24. Jin, H.; Dong, E.; Xu, M.; Liu, C.; Alici, G.; Jie, Y., Soft and smart modular structures actuated by shape memory alloy (SMA) wires as tentacles of soft robots. *Smart Materials and Structures* **2016,** *25* (8), 085026.

25. Chenal, T. P.; Case, J. C.; Paik, J.; Kramer, R. K. In *Variable stiffness fabrics with embedded shape memory materials for wearable applications*, 2014 IEEE/RSJ International Conference on Intelligent Robots and Systems, IEEE: 2014; pp 2827-2831.

26. Hawkes, E. W.; Blumenschein, L. H.; Greer, J. D.; Okamura, A. M., A soft robot that navigates its environment through growth. *Science Robotics* **2017,** *2* (8).

27. Tang, X.; Li, K.; Liu, Y.; Zhou, D.; Zhao, J., A general soft robot module driven by twisted and coiled actuators. *Smart Materials and Structures* **2019,** *28* (3), 035019.

28. Onal, C. D.; Rus, D., Autonomous undulatory serpentine locomotion utilizing body dynamics of a fluidic soft robot. *Bioinspiration & biomimetics* **2013,** *8* (2), 026003.

29. Morales, D.; Palleau, E.; Dickey, M. D.; Velev, O. D., Electro-actuated hydrogel walkers with dual responsive legs. *Soft matter* **2014,** *10* (9), 1337-1348.

30. Dreyfus, R.; Baudry, J.; Roper, M. L.; Fermigier, M.; Stone, H. A.; Bibette, J., Microscopic artificial swimmers. *Nature* **2005,** *437* (7060), 862-865.

31. Shepherd, R. F.; Stokes, A. A.; Freake, J.; Barber, J.; Snyder, P. W.; Mazzeo, A. D.; Cademartiri, L.; Morin, S. A.; Whitesides, G. M., Using explosions to power a soft robot. *Angewandte Chemie International Edition* **2013,** *52* (10), 2892-2896.

32. Joey, Z. G.; Calderón, A. A.; Chang, L.; Pérez-Arancibia, N. O., An earthworm-inspired friction-controlled soft robot capable of bidirectional locomotion. *Bioinspiration & biomimetics* **2019,** *14* (3), 036004.

33. Calderón, A. A.; Ugalde, J. C.; Zagal, J. C.; Pérez-Arancibia, N. O. In *Design, fabrication and control of a multi-material-multi-actuator soft robot inspired by burrowing worms*, 2016 IEEE international conference on robotics and biomimetics (ROBIO), IEEE: 2016; pp 31-38.

34. Laschi, C.; Cianchetti, M.; Mazzolai, B.; Margheri, L.; Follador, M.; Dario, P., Soft robot arm inspired by the octopus. *Advanced Robotics* **2012,** *26* (7), 709-727.

35. Li, T.; Nakajima, K.; Calisti, M.; Laschi, C.; Pfeifer, R. In *Octopus-inspired sensorimotor control of a multi-arm soft robot*, 2012 IEEE International Conference on Mechatronics and Automation, IEEE: 2012; pp 948-955.

36. Godaba, H.; Li, J.; Wang, Y.; Zhu, J., A soft jellyfish robot driven by a dielectric elastomer actuator. *IEEE Robotics and Automation Letters* **2016,** *1* (2), 624-631.

37. Frame, J.; Lopez, N.; Curet, O.; Engeberg, E. D., Thrust force characterization of free-swimming soft robotic jellyfish. *Bioinspiration & biomimetics* **2018,** *13* (6), 064001.

38. Barak, M., *Electrochemical power sources: primary and secondary batteries*. IET: 1980.

39. Takehara, Z.-i., Dissolution and precipitation reactions of lead sulfate in positive and negative electrodes in lead acid battery. *Journal of power sources* **2000,** *85* (1), 29-37.

40. Aubin, C. A.; Choudhury, S.; Jerch, R.; Archer, L. A.; Pikul, J. H.; Shepherd, R. F., Electrolytic vascular systems for energy-dense robots. *Nature* **2019,** *571* (7763), 51-57.

41. Kim, T.-H.; Lee, S.-J.; Choi, W. In *Design and control of the phase shift full bridge converter for the on-board battery charger of the electric forklift*, 8th International Conference on Power Electronics-ECCE Asia, IEEE: 2011; pp 2709-2716.

42. Liu, P.; Sherman, E.; Jacobsen, A., Design and fabrication of multifunctional structural batteries. *Journal of Power Sources* **2009,** *189* (1), 646-650.

43. Snyder, J. F.; Carter, R. H.; Wetzel, E. D., Electrochemical and mechanical behavior in mechanically robust solid polymer electrolytes for use in multifunctional structural batteries. *Chemistry of materials* **2007,** *19* (15), 3793-3801.

44. Renda, F.; Giorelli, M.; Calisti, M.; Cianchetti, M.; Laschi, C., Dynamic model of a multibending soft robot arm driven by cables. *IEEE Transactions on Robotics* **2014,** *30* (5), 1109-1122.

45. Umedachi, T.; Vikas, V.; Trimmer, B. A. In *Highly deformable 3-d printed soft robot generating inching and crawling locomotions with variable friction legs*, 2013 IEEE/RSJ international conference on Intelligent Robots and Systems, IEEE: 2013; pp 4590-4595.

46. Zhou, X.; Majidi, C.; O'Reilly, O. M., Soft hands: An analysis of some gripping mechanisms in soft robot design. *International Journal of Solids and Structures* **2015,** *64*, 155-165.

47. Cao, J.; Qin, L.; Liu, J.; Ren, Q.; Foo, C. C.; Wang, H.; Lee, H. P.; Zhu, J., Untethered soft robot capable of stable locomotion using soft electrostatic actuators. *Extreme Mechanics Letters* **2018,** *21*, 9-16.

48. Song, Y. S.; Sun, Y.; Van Den Brand, R.; Von Zitzewitz, J.; Micera, S.; Courtine, G.; Paik, J. In *Soft robot for gait rehabilitation of spinalized rodents*, 2013 IEEE/RSJ International Conference on Intelligent Robots and Systems, Ieee: 2013; pp 971-976.

49. Soloveichik, G. L., Flow batteries: current status and trends. *Chemical reviews* **2015,** *115* (20), 11533-11558.

50. Weber, A. Z.; Mench, M. M.; Meyers, J. P.; Ross, P. N.; Gostick, J. T.; Liu, Q., Redox flow batteries: a review. *Journal of applied electrochemistry* **2011,** *41* (10), 1137.

51. Weng, G.-M.; Li, Z.; Cong, G.; Zhou, Y.; Lu, Y.-C., Unlocking the capacity of iodide for high-energy-density zinc/polyiodide and lithium/polyiodide redox flow batteries. *Energy & Environmental Science* **2017,** *10* (3), 735-741.

52. Li, B.; Nie, Z.; Vijayakumar, M.; Li, G.; Liu, J.; Sprenkle, V.; Wang, W., Ambipolar zinc-polyiodide electrolyte for a high-energy density aqueous redox flow battery. *Nature communications* **2015,** *6*, 6303.

53. Janoschka, T.; Martin, N.; Martin, U.; Friebe, C.; Morgenstern, S.; Hiller, H.; Hager, M. D.; Schubert, U. S., An aqueous, polymer-based redox-flow battery using non-corrosive, safe, and low-cost materials. *Nature* **2015,** *527* (7576), 78-81.

54. Duduta, M.; Ho, B.; Wood, V. C.; Limthongkul, P.; Brunini, V. E.; Carter, W. C.; Chiang, Y. M., Semi-Solid lithium rechargeable flow battery. *Advanced Energy Materials* **2011,** *1* (4), 511-516.

55. De Leon, C. P.; Frías-Ferrer, A.; González-García, J.; Szánto, D.; Walsh, F. C., Redox flow cells for energy conversion. *Journal of power sources* **2006,** *160* (1), 716-732.

56. Thaller, L. H. In *Electrically rechargeable redox flow cells*, iece, 1974; pp 924-928.

57. Badwal, S. P.; Giddey, S. S.; Munnings, C.; Bhatt, A. I.; Hollenkamp, A. F., Emerging electrochemical energy conversion and storage technologies. *Frontiers in chemistry* **2014,** *2*, 79.

58. Alotto, P.; Guarnieri, M.; Moro, F., Redox flow batteries for the storage of renewable energy: A review. *Renewable and Sustainable Energy Reviews* **2014,** *29*, 325-335.

59. Aaron, D.; Sun, C.-N.; Bright, M.; Papandrew, A. B.; Mench, M. M.; Zawodzinski Jr, T. A., In situ kinetics studies in all-vanadium redox flow batteries. *ECS Electrochemistry Letters* **2013,** *2* (3), A29.

60. Arenas, L.; De León, C. P.; Walsh, F., Engineering aspects of the design, construction and performance of modular redox flow batteries for energy storage. *Journal of Energy Storage* **2017,** *11*, 119-153.

61. Zhao, P.; Zhang, H.; Zhou, H.; Chen, J.; Gao, S.; Yi, B., Characteristics and performance of 10 kW class all-vanadium redox-flow battery stack. *Journal of Power Sources* **2006,** *162* (2), 1416-1420.

62. Wang, Q.; Qu, Z.; Jiang, Z.; Yang, W., Experimental study on the performance of a vanadium redox flow battery with non-uniformly compressed carbon felt electrode. *Applied Energy* **2018,** *213*, 293-305.

63. Pellegri, A.; Broman, B. M., Redox flow battery system and cell stack. Google Patents: 2002.

64. Lai, Q.; Zhang, H.; Li, X.; Zhang, L.; Cheng, Y., A novel single flow zinc–bromine battery with improved energy density. *Journal of Power Sources* **2013,** *235*, 1-4.

65. Zhang, L.; Zhang, H.; Lai, Q.; Li, X.; Cheng, Y., Development of carbon coated membrane for zinc/bromine flow battery with high power density. *Journal of power sources* **2013,** *227*, 41-47.

66. Wu, M.; Zhao, T.; Jiang, H.; Zeng, Y.; Ren, Y., High-performance zinc bromine flow battery via improved design of electrolyte and electrode. *Journal of Power Sources* **2017,** *355*, 62-68.

67. Carr, P.; Symons, P. C.; Aller, D. J., Operational zinc chlorine battery based on a water store. Google Patents: 1979.

68. Whittlesey, C. C.; Mashikian, M. S., Zinc-chlorine battery plant system and method. Google Patents: 1981.

69. Jorné, J.; Kim, J.; Kralik, D., The zinc-chlorine battery: half-cell overpotential measurements. *Journal of Applied Electrochemistry* **1979,** *9* (5), 573-579.

70. Xie, Z.; Liu, Q.; Chang, Z.; Zhang, X., The developments and challenges of cerium half-cell in zinc–cerium redox flow battery for energy storage. *Electrochimica Acta* **2013,** *90*, 695-704.

71. Leung, P.; De León, C. P.; Walsh, F., An undivided zinc–cerium redox flow battery operating at room temperature (295 K). *Electrochemistry Communications* **2011,** *13* (8), 770-773.

72. Cheng, J.; Zhang, L.; Yang, Y.-S.; Wen, Y.-H.; Cao, G.-P.; Wang, X.-D., Preliminary study of single flow zinc–nickel battery. *Electrochemistry Communications* **2007,** *9* (11), 2639-2642.

73. Ito, Y.; Nyce, M.; Plivelich, R.; Klein, M.; Steingart, D.; Banerjee, S., Zinc morphology in zinc–nickel flow assisted batteries and impact on performance. *Journal of Power Sources* **2011,** *196* (4), 2340-2345.

74. Zhou, H.; Zhang, H.; Zhao, P.; Yi, B., A comparative study of carbon felt and activated carbon based electrodes for sodium polysulfide/bromine redox flow battery. *Electrochimica Acta* **2006,** *51* (28), 6304-6312.

75. Zhao, P.; Zhang, H.; Zhou, H.; Yi, B., Nickel foam and carbon felt applications for sodium polysulfide/bromine redox flow battery electrodes. *Electrochimica Acta* **2005,** *51* (6), 1091-1098.

76. Zeng, Y.; Zhao, T.; An, L.; Zhou, X.; Wei, L., A comparative study of all-vanadium and iron-chromium redox flow batteries for large-scale energy storage. *Journal of Power Sources* **2015,** *300*, 438-443.

77. Zeng, Y.; Zhou, X.; An, L.; Wei, L.; Zhao, T., A high-performance flow-field structured iron-chromium redox flow battery. *Journal of Power Sources* **2016,** *324*, 738-744.

78. Ding, C.; Zhang, H.; Li, X.; Liu, T.; Xing, F., Vanadium flow battery for energy storage: prospects and challenges. *The journal of physical chemistry letters* **2013,** *4* (8), 1281-1294.

79. Yao, C.; Zhang, H.; Liu, T.; Li, X.; Liu, Z., Carbon paper coated with supported tungsten trioxide as novel electrode for all-vanadium flow battery. *Journal of Power Sources* **2012,** *218*, 455-461.

80. Sun, B.; Skyllas-Kazakos, M., Chemical modification and electrochemical behaviour of graphite fibre in acidic vanadium solution. *Electrochimica Acta* **1991,** *36* (3-4), 513-517.

81. Sum, E.; Skyllas-Kazacos, M., Dissolution study of electrolytically deposited aluminium at a graphite electrode. *Electrochimica acta* **1991,** *36* (5-6), 811-817.

82. Chakrabarti, M.; Brandon, N.; Hajimolana, S.; Tariq, F.; Yufit, V.; Hashim, M.; Hussain, M.; Low, C.; Aravind, P., Application of carbon materials in redox flow batteries. *Journal of Power Sources* **2014,** *253*, 150-166.

83. Zhong, S.; Kazacos, M.; Burford, R.; Skyllas-Kazacos, M., Fabrication and activation studies of conducting plastic composite electrodes for redox cells. *Journal of power sources* **1991,** *36* (1), 29-43.

84. Chang, T.-C.; Zhang, J.-P.; Fuh, Y.-K., Electrical, mechanical and morphological properties of compressed carbon felt electrodes in vanadium redox flow battery. *Journal of Power Sources* **2014,** *245*, 66-75.

85. Bromberger, K.; Kaunert, J.; Smolinka, T., A model for all-vanadium redox flow batteries: introducing electrode-compression effects on voltage losses and hydraulics. *Energy Technology* **2014,** *2* (1), 64-76.

86. Chi, P.-H.; Chan, S.; Weng, F.; Su, A.; Sui, P.; Djilali, N., On the effects of non-uniform property distribution due to compression in the gas diffusion layer of a PEMFC. *International Journal of Hydrogen Energy* **2010,** *35* (7), 2936-2948.